Supplementary Information for Observations of VOC emissions and chemical products over US oil- and gas-producing regions using high-resolution H_3O^+ CIMS (PTR-ToF-MS)

Abigail Koss[1,2,3], Bin Yuan[1,2, †], Carsten Warneke[1,2], Jessica B. Gilman[1], Brian M. Lerner[1,2*], Patrick R. Veres[1,2], Jeff Peischl[1,2], Scott Eilerman[1,2], Rob Wild[1,2], Steven S. Brown[1,3], Chelsea R. Thompson[1,2], Thomas Ryerson[1], Thomas Hanisco[4], Glenn Wolfe[4,5], Jason M. St. Clair[4,5], Mitchell Thayer[6], Frank N. Keutsch[6,7], Shane Murphy[8], Joost de Gouw[2,3]

1. NOAA Earth System Research Laboratory (ESRL), Chemical Sciences Division, Boulder, CO, USA

2. Cooperative Institute for Research in Environmental Sciences, University of Colorado at Boulder, Boulder, CO, USA

3. Department of Chemistry and Biochemistry, University of Colorado at Boulder, CO, USA

4. NASA Goddard Space Flight Center, Greenbelt, MD, USA

5. University of Maryland Baltimore County, Baltimore, MD, USA

6. University of Wisconsin Madison, Madison, WI, USA

7. Paulson School of Engineering and Applied Sciences and Department of Chemistry and Chemical Biology, Harvard University, Cambridge, MA, USA

8. University of Wyoming, Laramie, WY, USA

† now at now at Laboratory of Atmospheric Chemistry, Paul Scherrer Institute, 5232 Villigen, Switzerland

* now at Aerodyne Research, Inc., Billerica, MA, USA

S1. Peak fitting errors: data quality assessment

At the resolution of the H_3O^+ ToF CIMS instrument (~4000 m/dm), peaks at the same nominal mass frequently overlap. To separate the contribution from overlapping peaks at the same nominal mass, the Tofware peak fitting software (Aerodyne Resarch Inc./Tofwerk AG) iteratively fits a set of pseudo-gaussian high-resolution peaks to the sum signal across that nominal mass. The number of peaks at a given nominal mass, the peak shape, and the exact m/z of each peak center are user-defined. However, problems can occur in circumstances where a peak is much smaller than its neighbor, or where the m/z separation between peaks is unusually small. Under these circumstances, the returned peak-fit intensity can be highly inaccurate. The magnitude of the error depends on the relative size, closeness in m/z space, mass calibration precision and accuracy, and peak shape of the overlapping peak, and so it can change over time. These nonrandom errors can create false variability in a particular ion mass. This peak fitting issue is well known for both CISM and AMS instruments but has not yet been completely addressed (Müller et al., 2011;Cubison and Jimenez, 2015;Stark et al., 2015;Corbin et al., 2015).

Although there is not yet a quantitative method to determine the extent and magnitude of peak overlap errors in every situation, Tofware provides qualitative assessment tools that rely on the dependence of peak-fitting error on mass calibration precision (Timonen et al., 2016). Several studies have suggested that mass calibration precision and accuracy are strong controls on peak fitting error (Corbin et al., 2015;Cubison and Jimenez, 2015). When applied to a particular high-resolution peak, the tool re-calculates the fitted peak intensity for a range of expected error in the mass calibration (±10 ppm). Peaks that are strongly affected by peak overlap error will have highly variable fitted peak intensity. All high-resolution peaks reported in this work are not strongly affected by peak fit error, i.e., the fitted peak intensity is independent of mass calibration uncertainty. Mass spectra and time-series fitted with mass calibration ±10 ppm are shown in Figure SI 4.

S2. Limit of detection calculation

The measured instrument signal (ion counts) is the product of the measurement time t, the sensitivity C_f, and the concentration $[X]$:

$$S = C_f[X]t$$

Instrument noise is related to the square root of the signal:

$$N = \sqrt{S} = \sqrt{C_f[X]t}$$

The signal to noise ratio is therefore:

$$\frac{S}{N} = \frac{C_f[X]t}{\sqrt{C_f[X]t}} = \sqrt{C_f[X]t}$$

We define the "limit of detection" as the concentration $[X]$ at which the signal to noise ratio (S/N) equals 3:

$$\frac{S}{N} = 3 = \sqrt{C_f [X]_{LOD} t}$$

By solving for $[X]_{LoD}$, it can be seen that the limit of detection is inversely proportional to the measurement time:

$$[X]_{LoD} = \frac{9}{C_f t}$$

This is different from *noise*, which decreases as the square root of the measurement time.

For several reasons, the measurement limit of detection is actually somewhat higher than the calculations above would suggest. First, there is some background count rate B, and the VOC signal is determined from the difference between the ambient signal and the background signal. Second, because of additional error from high-resolution peak fitting, the noise is somewhat higher than the square root of the signal. To account for this additional error, a linear scaling factor α is included in the calculation of noise. With the inclusion of the background B and scaling factor α, the signal to noise calculation is (Bertram et al., 2011):

$$\frac{S}{N} = \frac{C_f [X] t}{\alpha \times \sqrt{C_f [X] t + 2Bt}} = 3$$

The detection limit $[X]$ can then be solved for using the quadratic equation. Detection limits given in this work were calculated using raw counts-per-second, without reagent ion normalization or a ToF duty-cycle correction applied.

S3. Photochemical aging analysis
The relative ratios of different VOCs can be used to establish relative photochemical aging. Using PTRMS measurements of C6-C10 aromatic species, this method has been applied to photochemical aging of VOCs in urban areas (de Gouw et al., 2005;Warneke et al., 2007) and in an oil and gas producing region (Koss et al., 2015). Benzene (C6 aromatic), has the slowest reaction rate with OH; as the cumulative OH exposure of an air mass increases, the ratios of other aromatics to benzene should decrease. The ratio of an aromatic VOC to benzene at time t can be written as:

$$\left(\frac{VOC}{Benzene}\right)_t = \left(\frac{VOC}{Benzene}\right)_0 \times e^{((k_{benzene} - k_{VOC}) \int_0^t [OH] dt)}$$

Where $\left(\frac{VOC}{Benzene}\right)_0$ is the ratio of the aromatic to benzene at time t=0, $k_{benzene}$ and k_{VOC} are the rate constants of benzene and the aromatic with OH, and $\int_0^t [OH] dt$ is the integrated OH exposure. If the ratio at time t, the emission ratio, and the OH rate constants are known, the integrated OH exposure can be calculated.
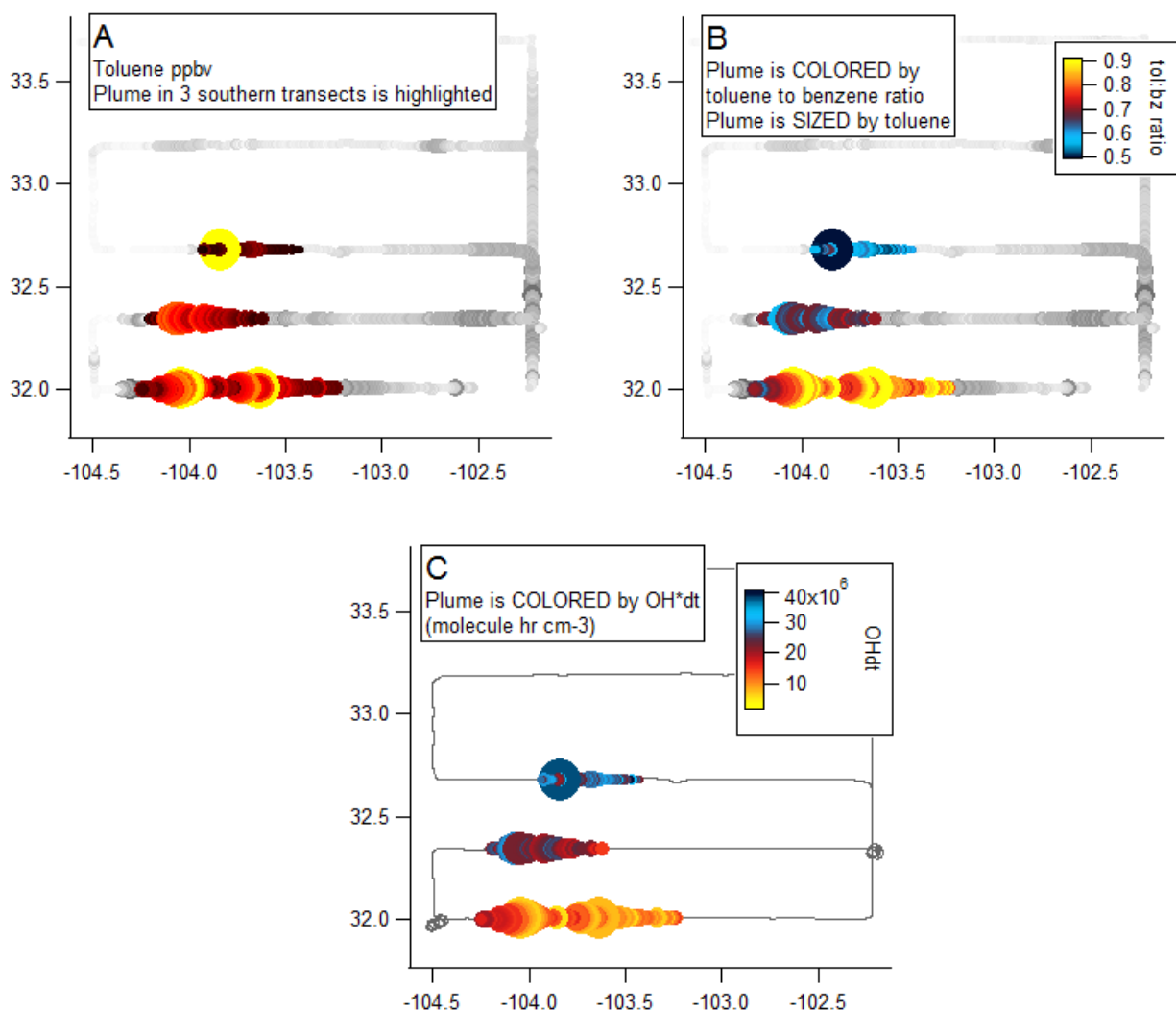
Figure SI 1. Aromatics and photochemical aging in the southwest section of the flight survey. (a) concentration of toluene. (b) ratio of toluene to benzene. (c) integrated OH exposure. In the highlighted (colored) section of the flight track, the markers are sized and colored by the integrated OH exposure.

We restricted this analysis to the three plume transects in the southwest portion of the flight survey. These three plumes have similar VOC composition, are located close to one another, and can be reasonably be assumed to be the same air mass. The flight was from south to north, so the northmost transect was latest in the day. The ratios of C7-C10 aromatics decrease from south to north (Figure SI 1).

We calculated integrated OH exposure in each of the three transects using toluene, C8 aromatics, C9 aromatics, and C10 aromatics. OH rate constants for C8, C9, and C10 aromatics were taken from Koss et al. (2015). OH rate constants for benzene and toluene were taken from Atkinson and Arey (2003). The average of the highest 5% points in the southmost transect was used as the ratio at time t=0. We note that in this analysis, time t=0 is not necessarily the time of emission. We set time t=0 to be the age of the least aged air mass. The exact emission ratio is not relevant

to the analysis of pyrrole presented in the manuscript, since we are mainly interested in the relative rate of aging.

The calculated OH exposures from C7-C10 aromatics were averaged to give the final OH exposure used in the analysis. The separately calculated OH exposures were within 40% of the mean.

The OH rate constant for pyrroline was calculated using an exponential best fit to the pyrroline:benzene ratio as a function of the integrated OH exposure.
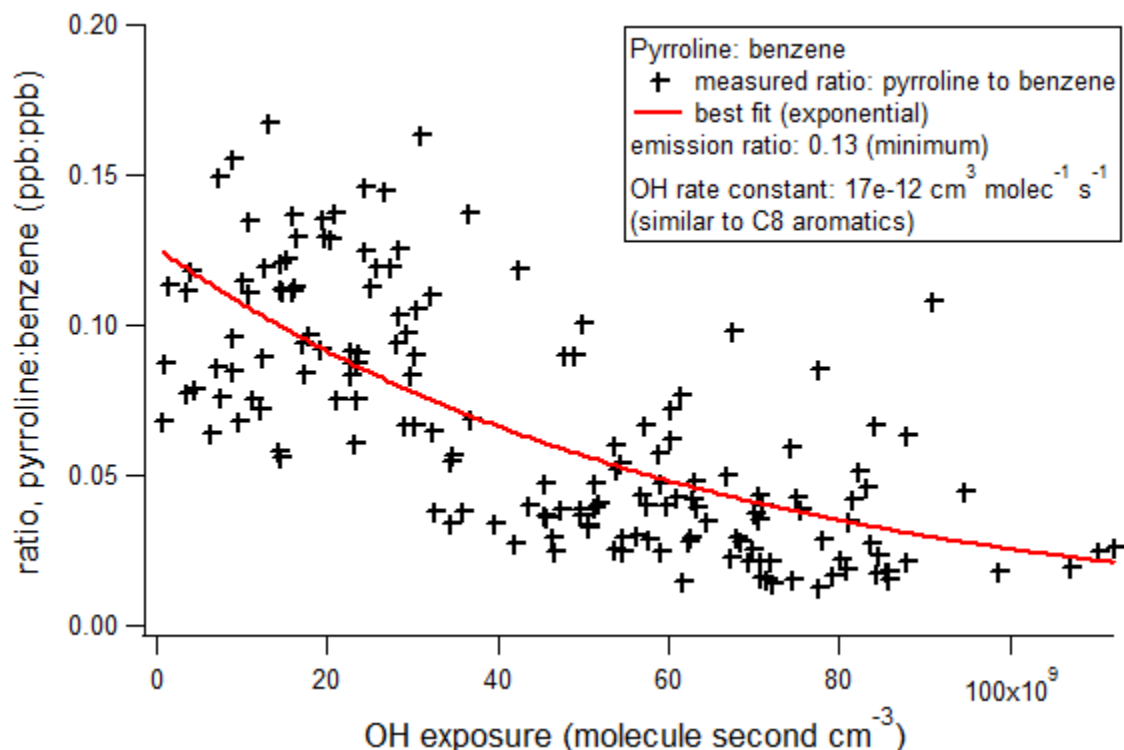
Figure SI2. Ratio of pyrroline to benzene as a function of OH exposure.

A sensitivity analysis for the calculated pyrroline OH rate constant is given below:

	OH rate constant, cm^3 cmolecule^{-1} s^{-1}	Emission ratio pyrroline:benzene
Original calculation	$1.72 \pm 0.14 \times 10^{-11}$	0.126 ± 0.006
Using maximum OHdt calculated from all aromatics	$1.39 \pm 0.11 \times 10^{-11}$	0.142 ± 0.008
Using minimum OHdt calculated from all aromatics	$1.78 \pm 0.17 \times 10^{-11}$	0.096 ± 0.004
Actual concentration 2x lower	$1.72 \pm 0.14 \times 10^{-11}$	0.252 ± 0.012
Actual concentration 2x higher	$1.72 \pm 0.14 \times 10^{-11}$	0.063 ± 0.003

Figure SI 3
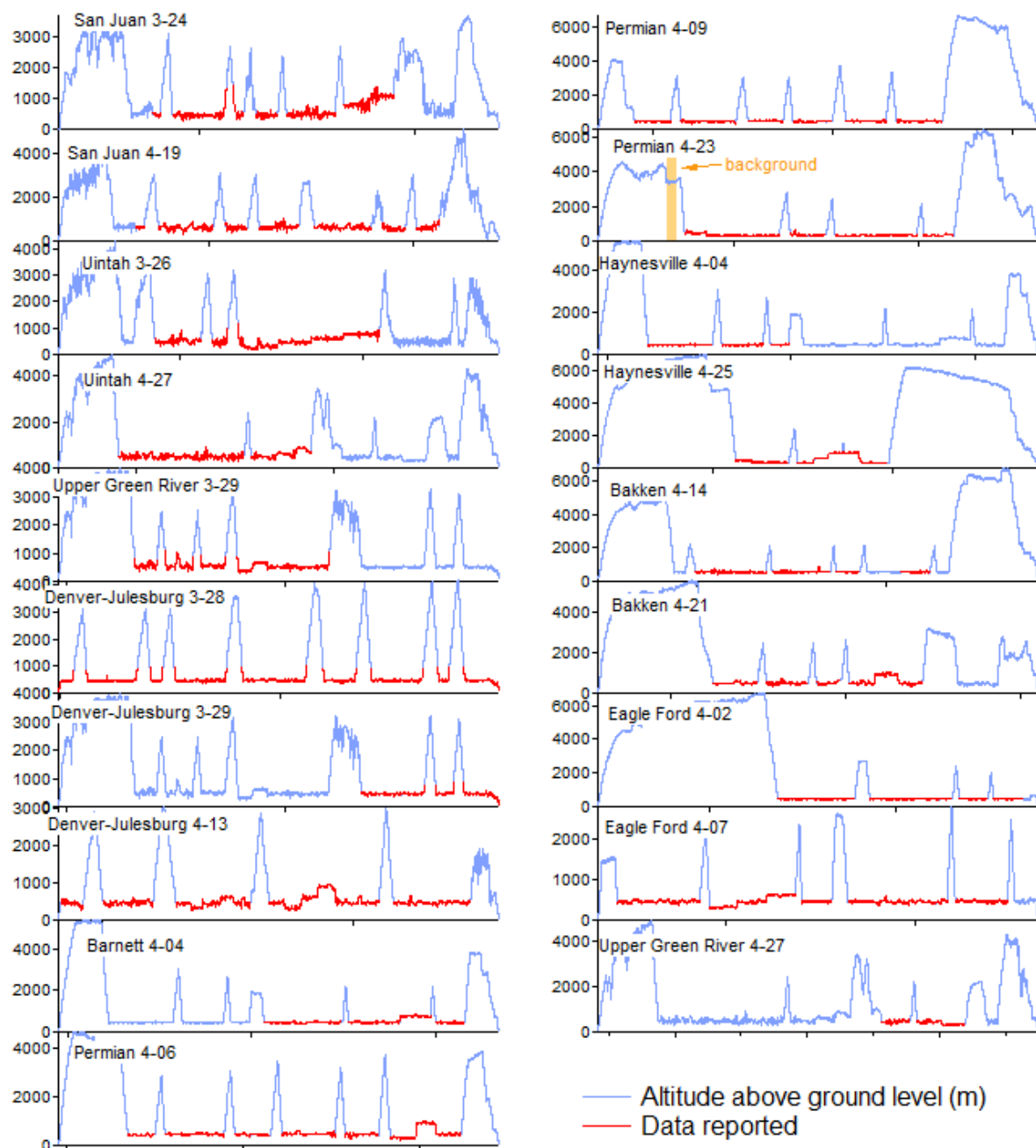
Data selection based on flight altitude for each flight.

Figure SI 4
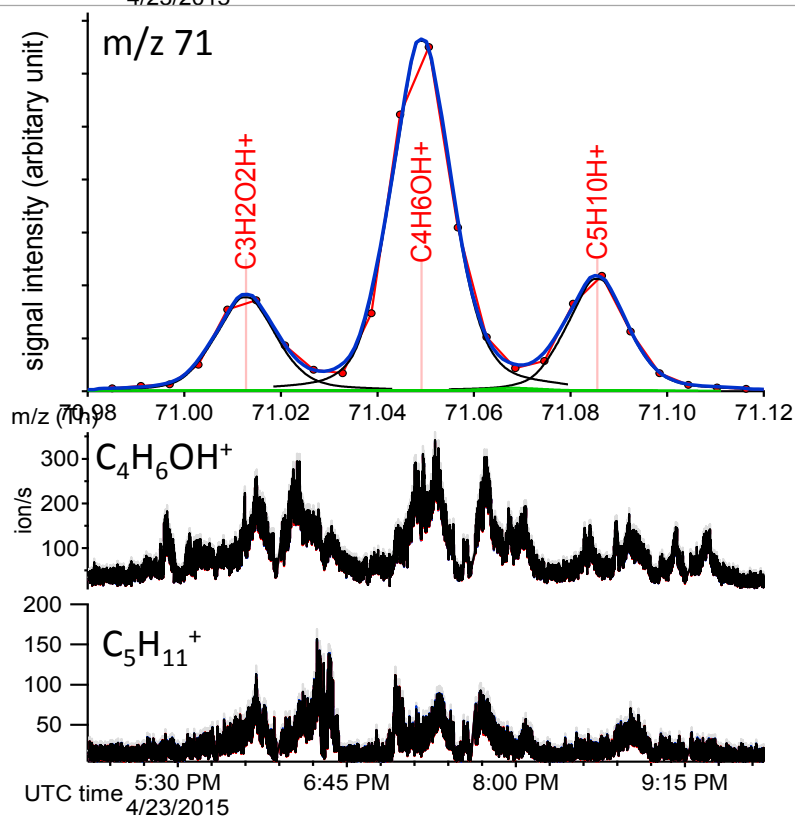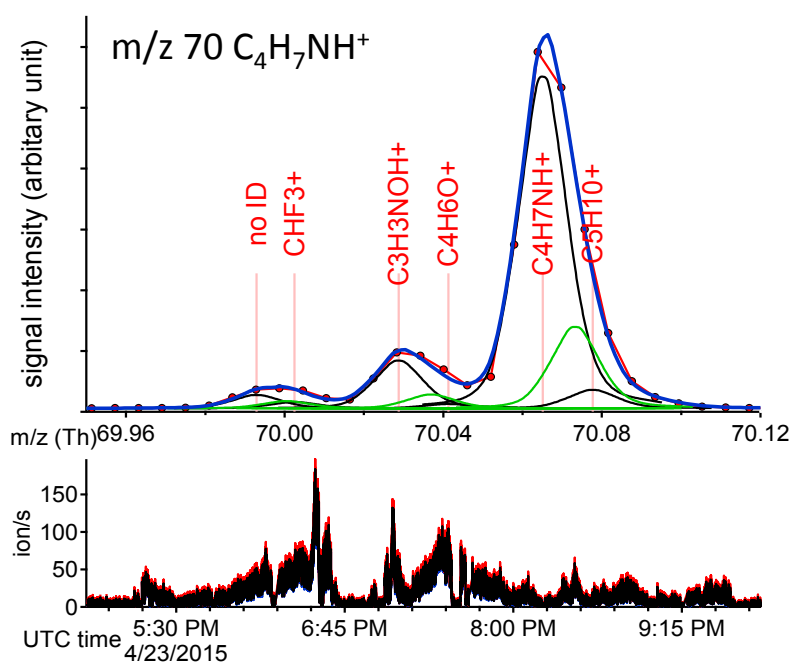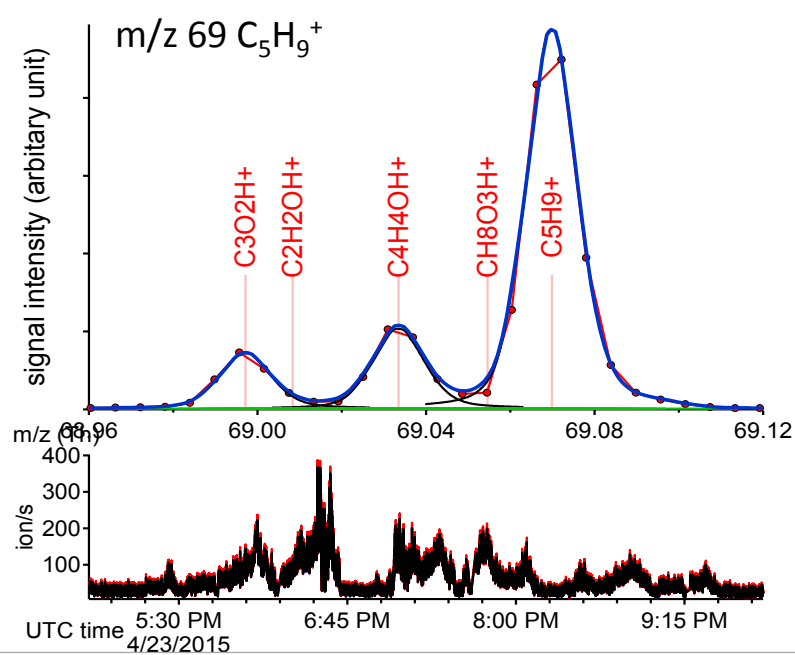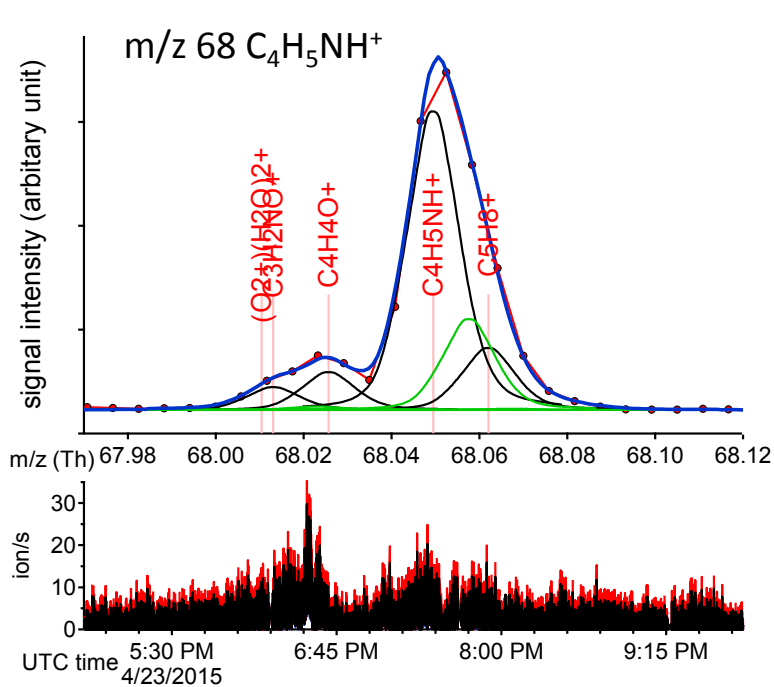
High-resolution mass spectra for select nominal masses.

Key:

Mass spectra

— sum HR fit
— measurement
— isotopes
— HR masses

Time series

— Reported fit
— Fit +10 ppm m/z cal
— Fit -10 ppm m/z cal

m/z 135 $C_{10}H_{14}H^+$

C2ClF4+
C4ClH3O3H+
C4H6O3SH+
C4H6O5H+
C8H8O2H+
C5H10O4H+
C9H10OH+
C6H14O3H+
C10H14H+

m/z 137 $C_{10}H_{16}H^+$

CrO4H5+
C7H4OSH+
C7H4O3H+
C8H8O2H+
C9H12OH+
C10H16H+

m/z 151 $C_{11}H_{18}H^+$

C4H6O6H+
C8H6O3H+
C5H10O5H+
C9H10O2H+
C6H14O4H+
C10H14OH+
C11H18H+
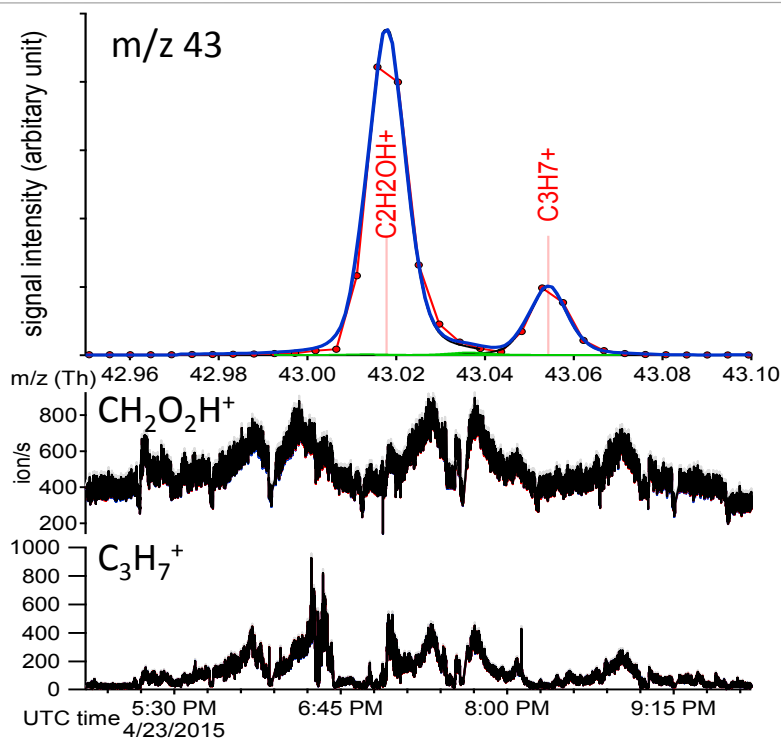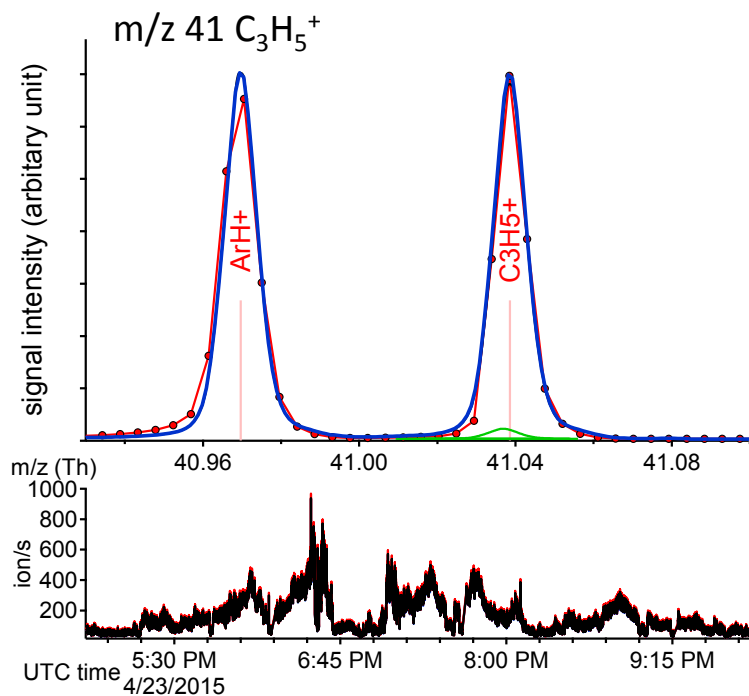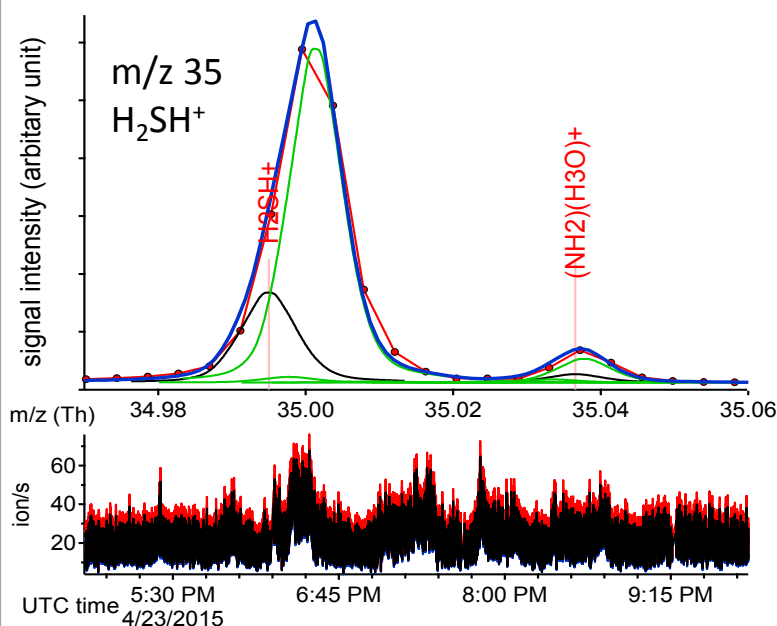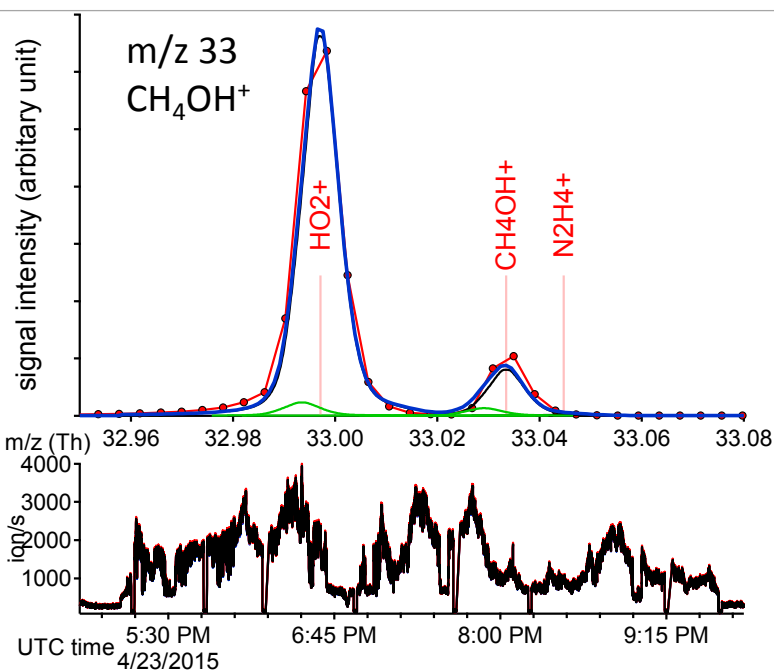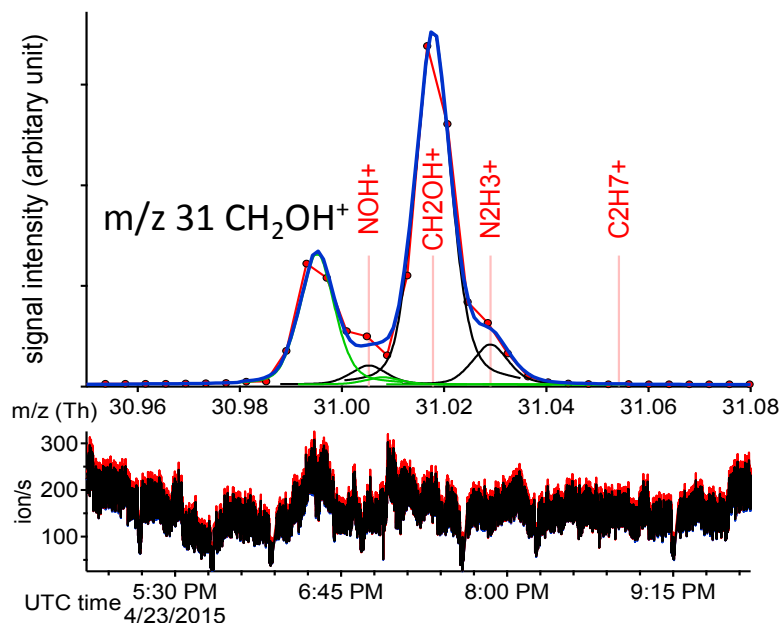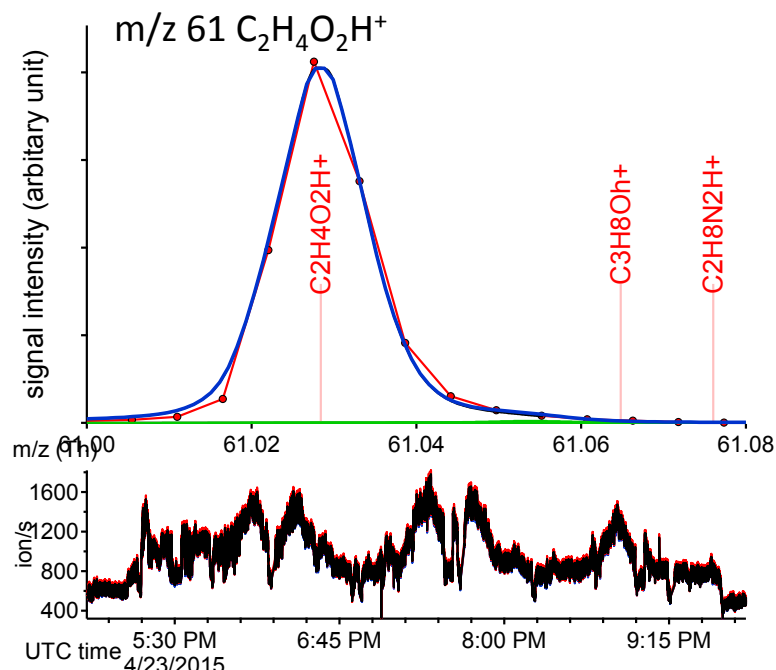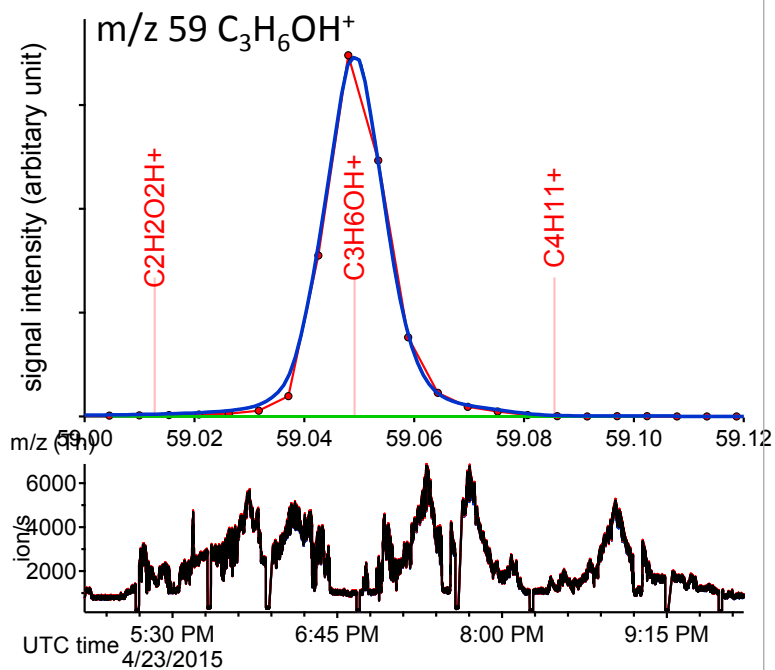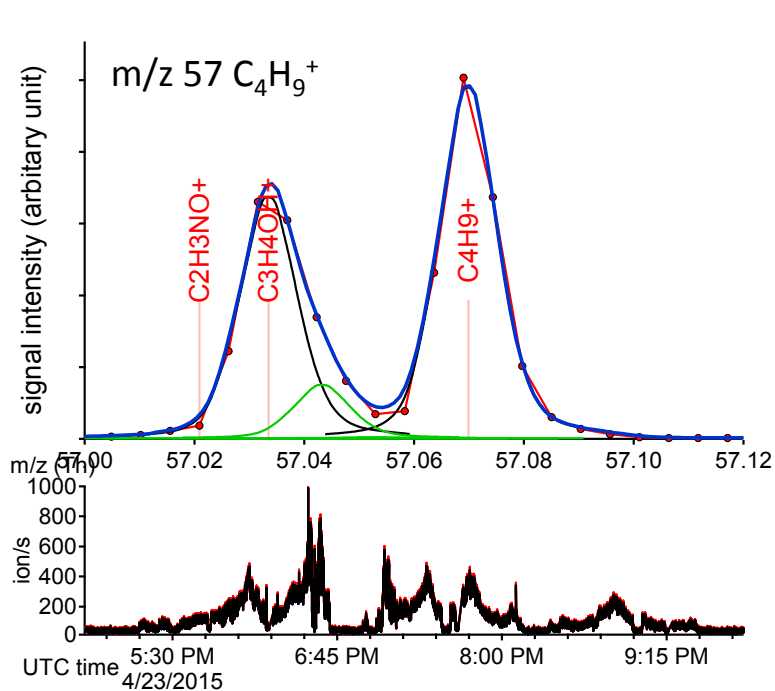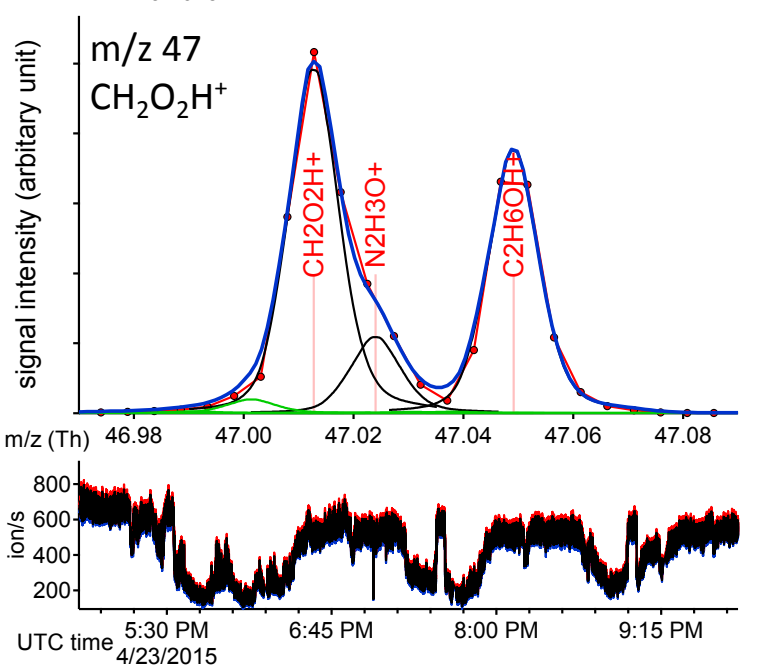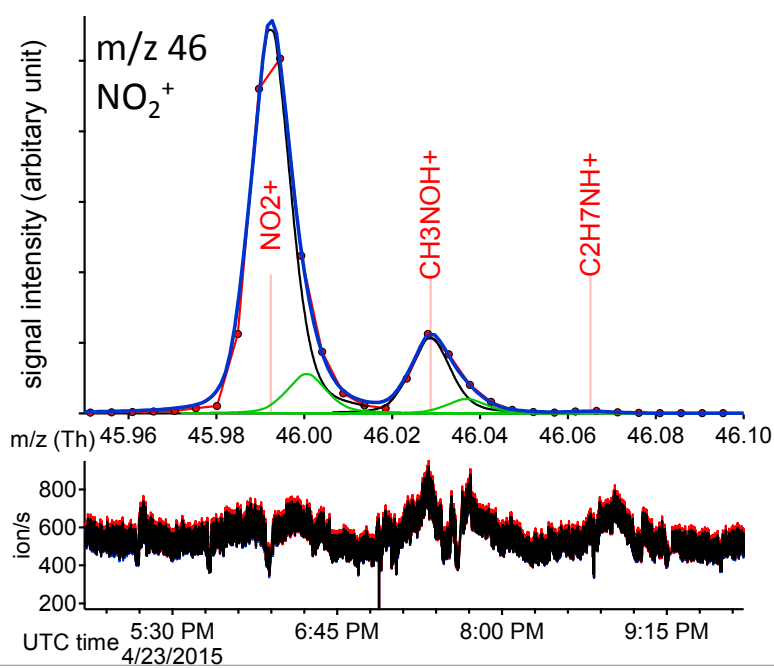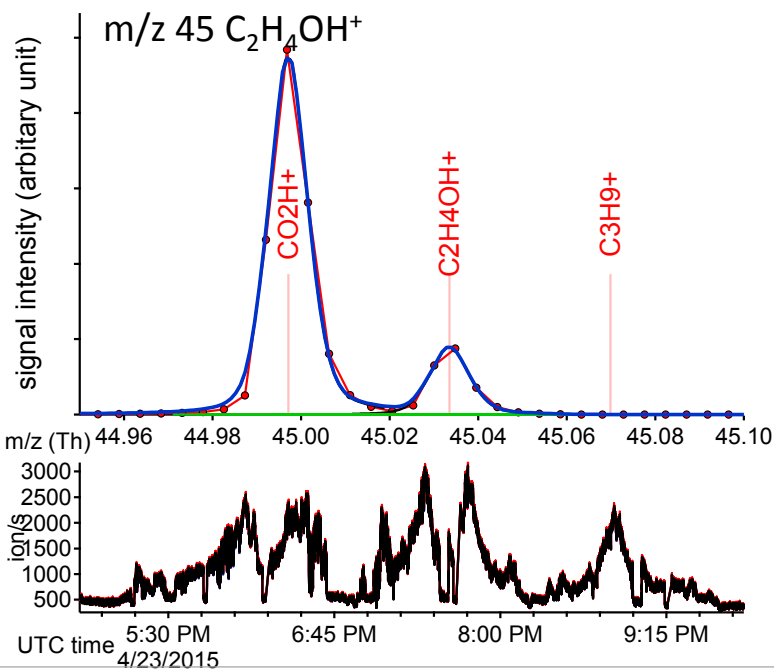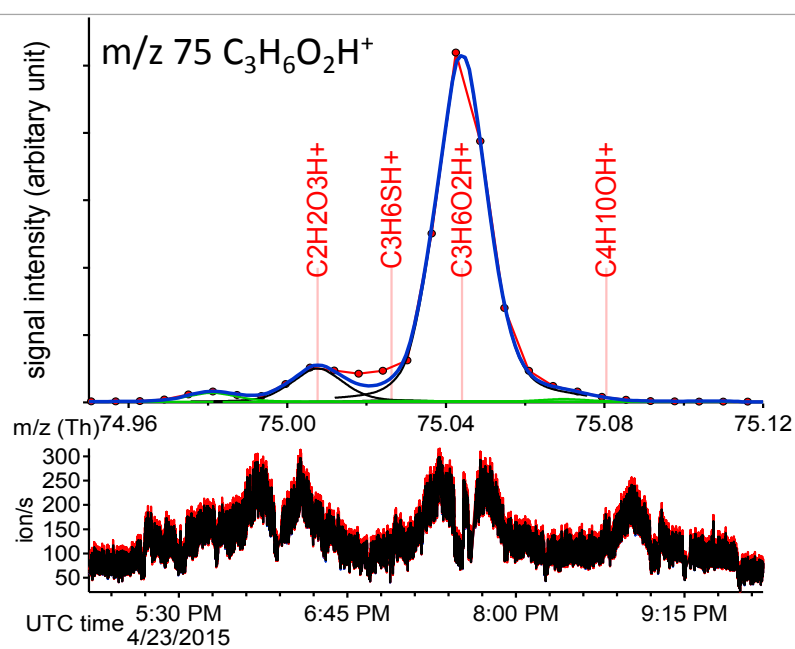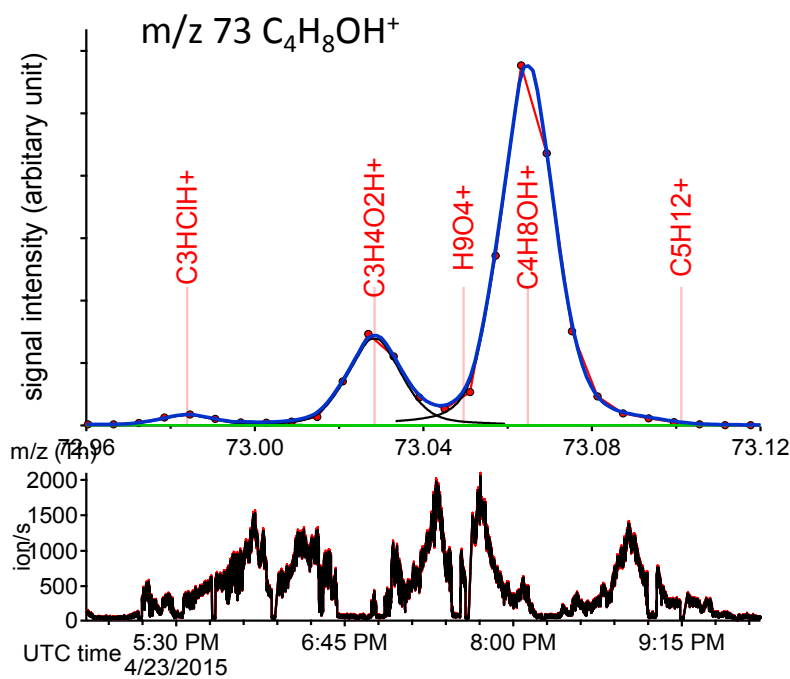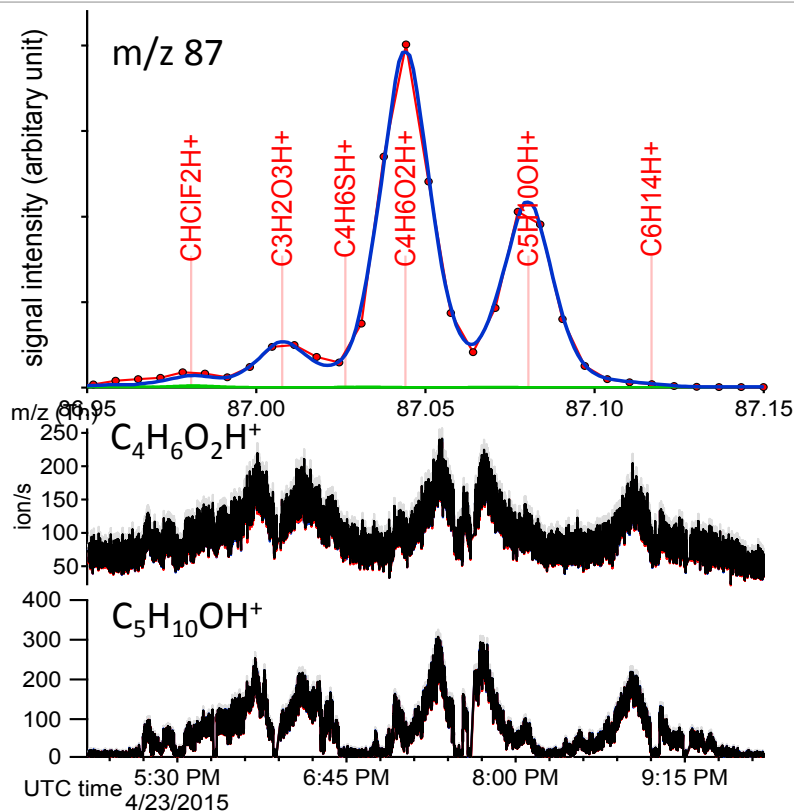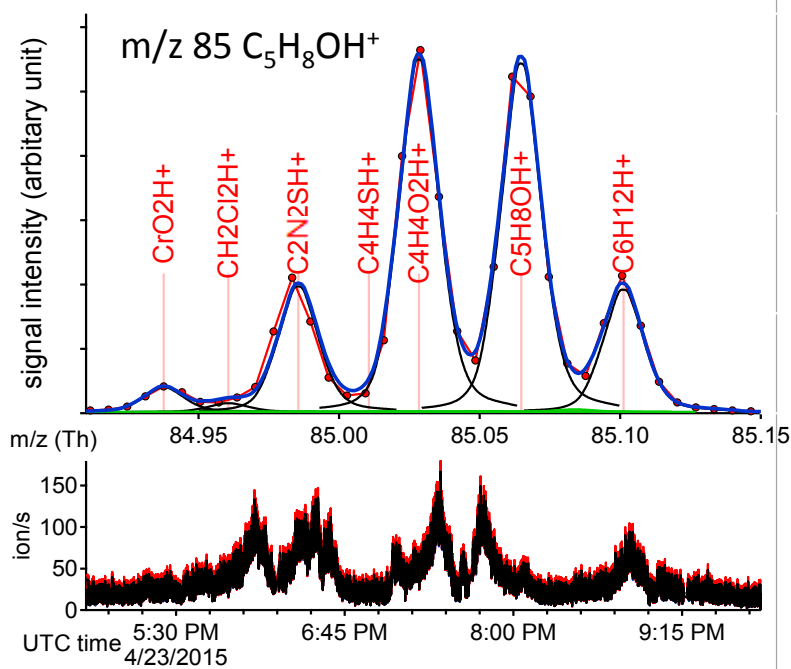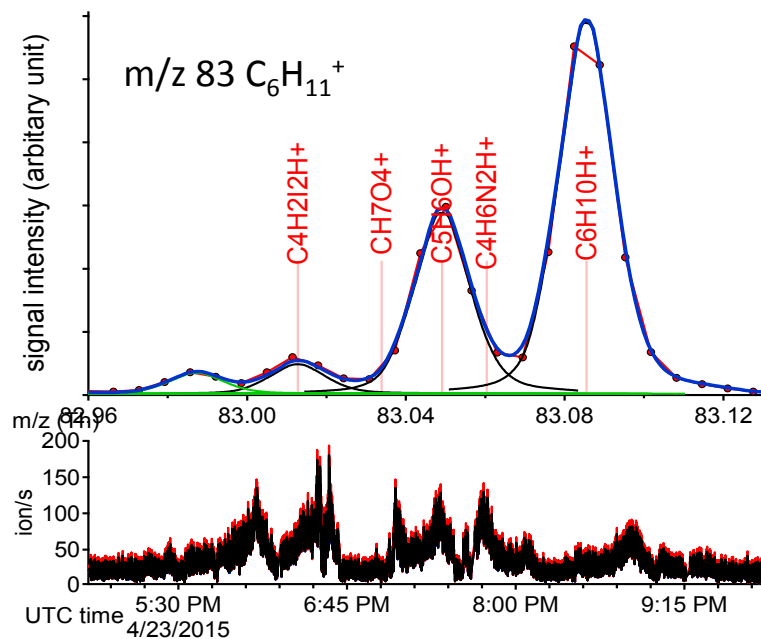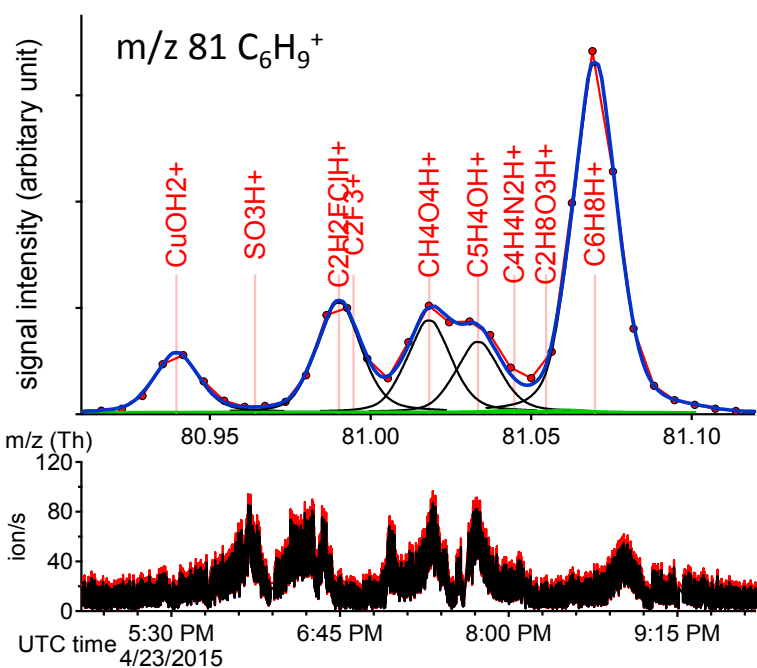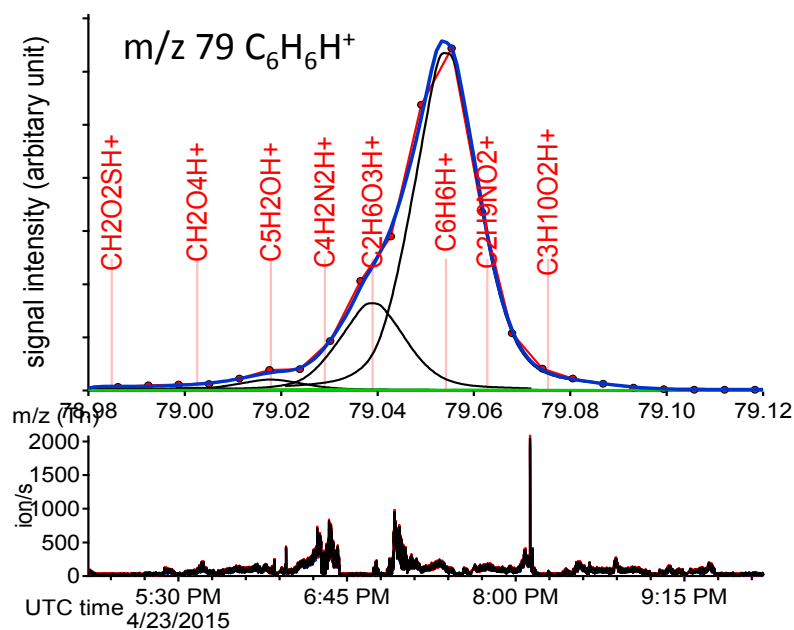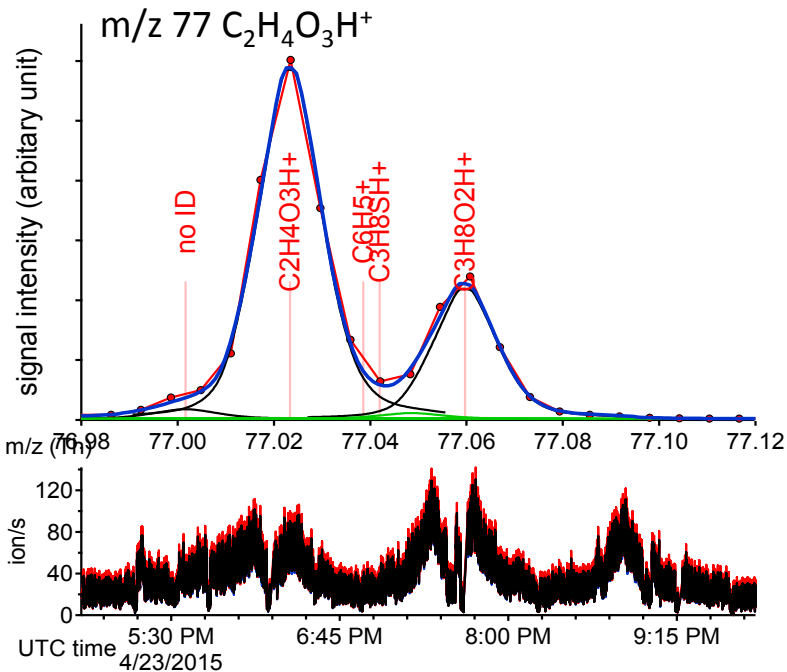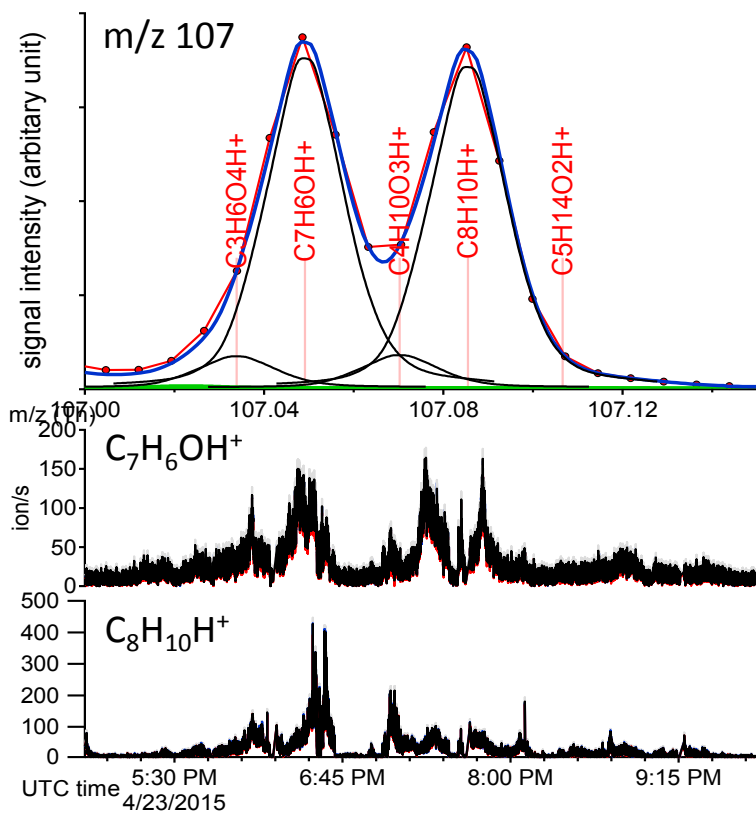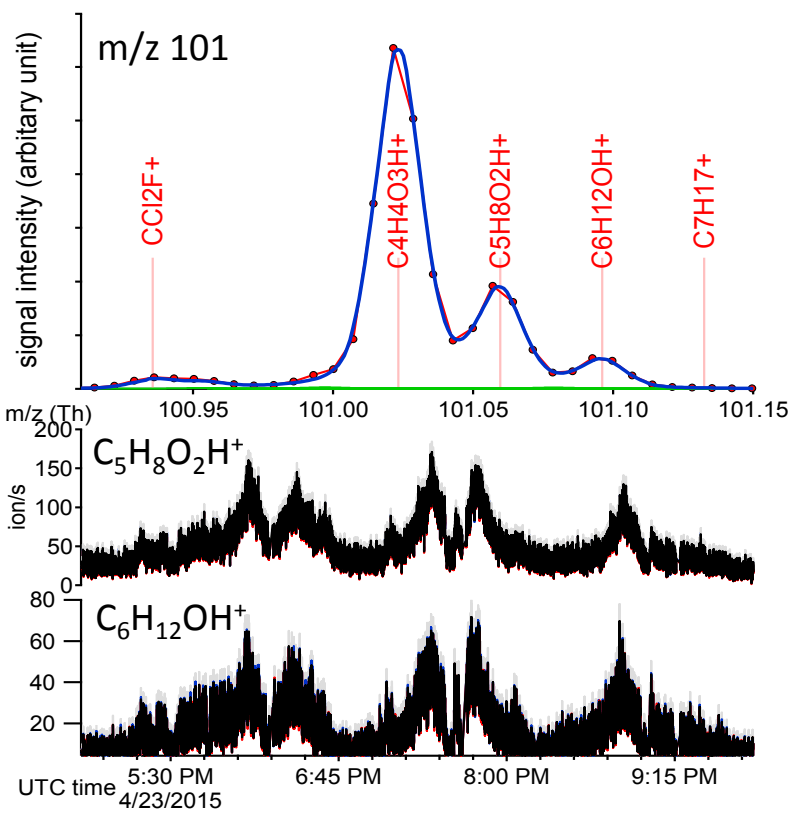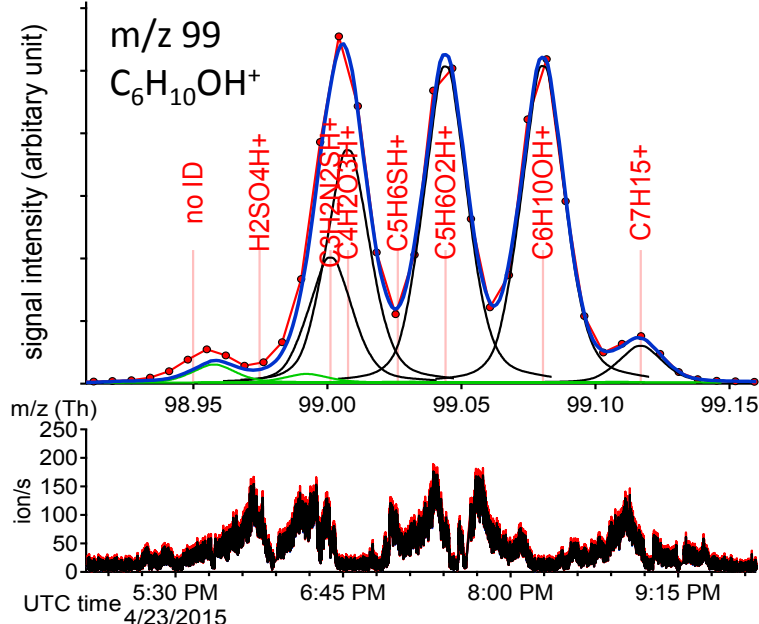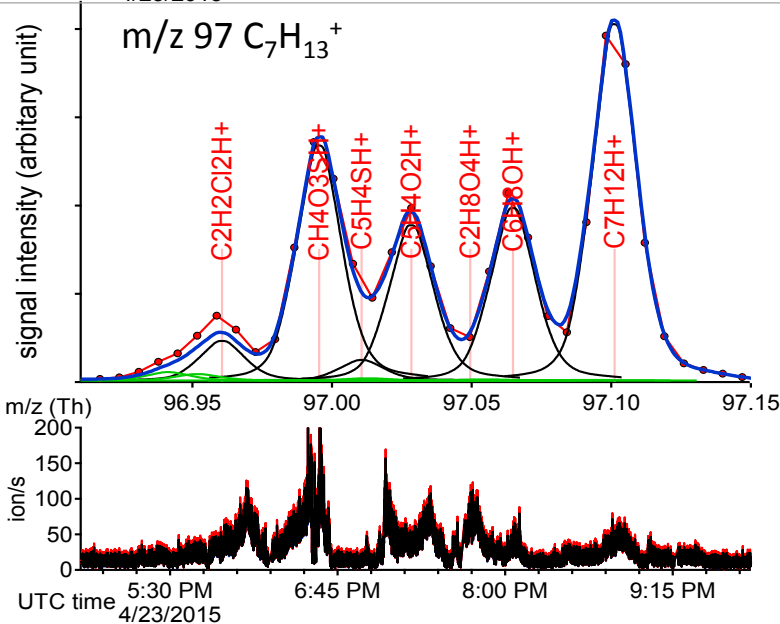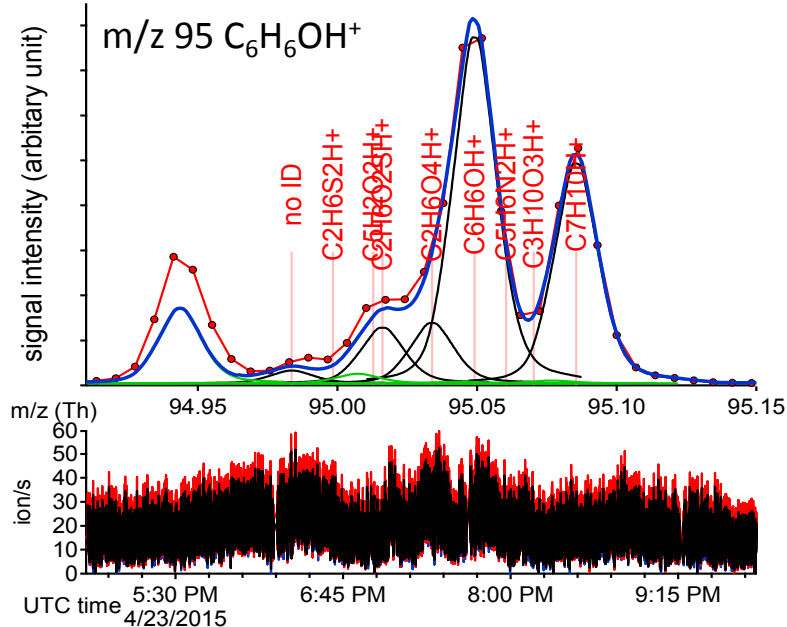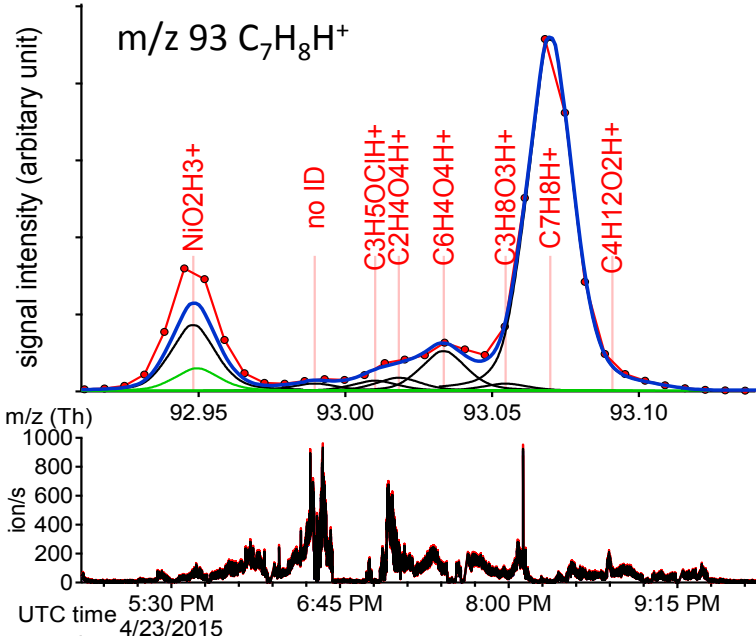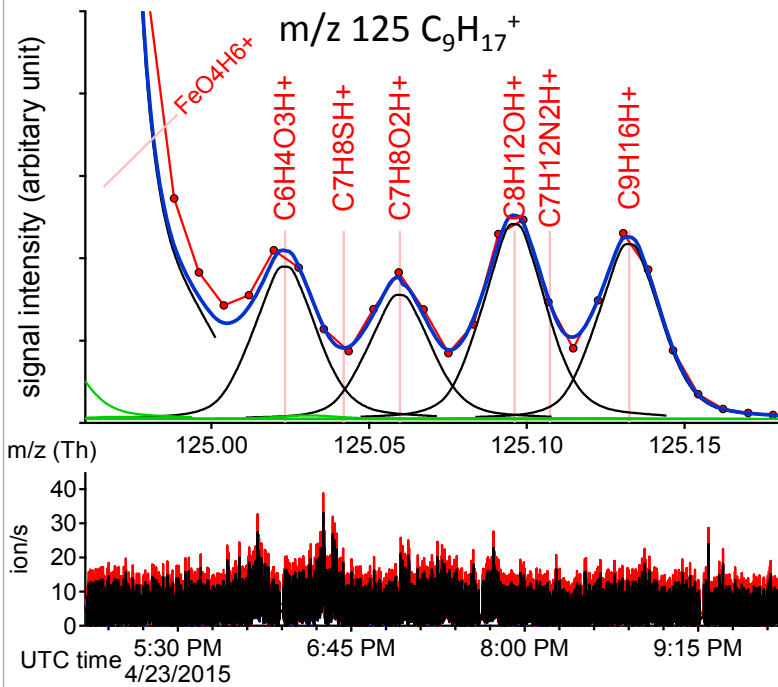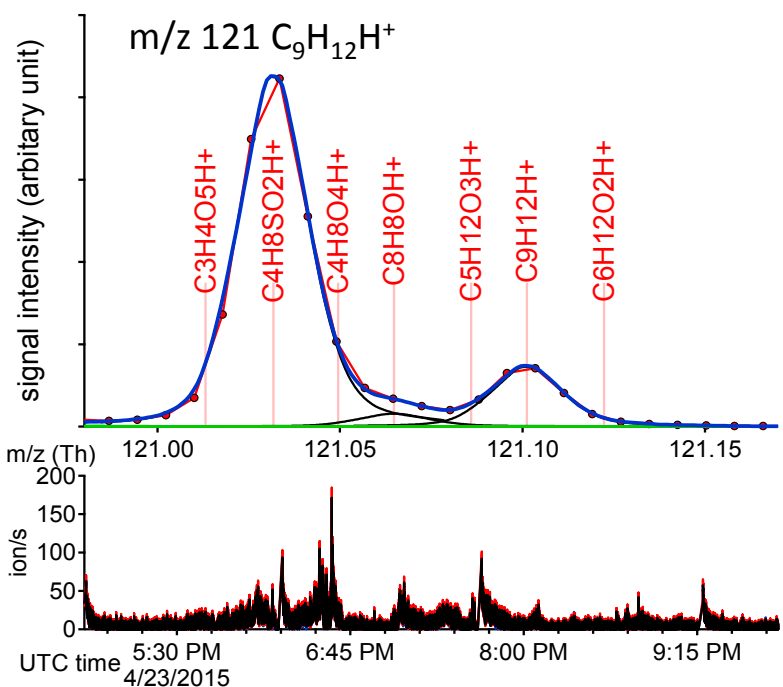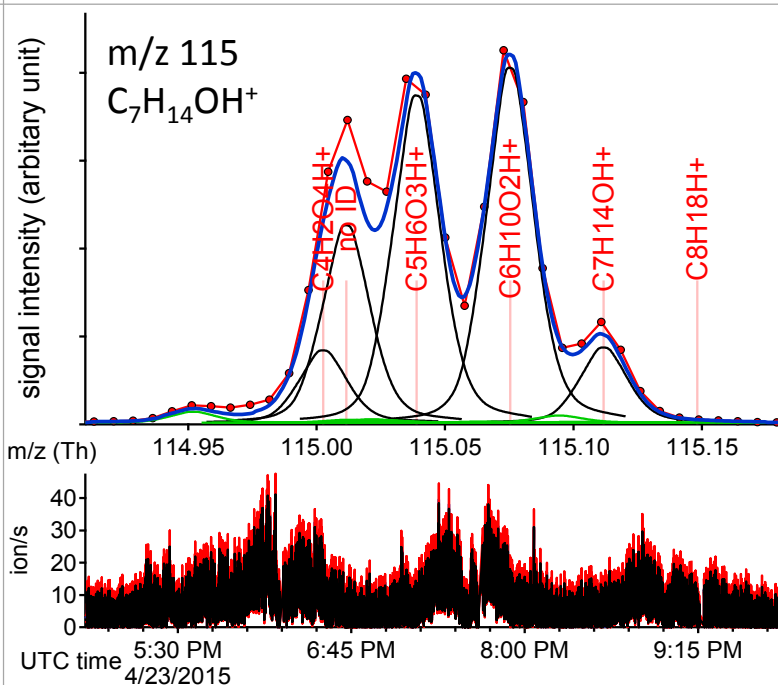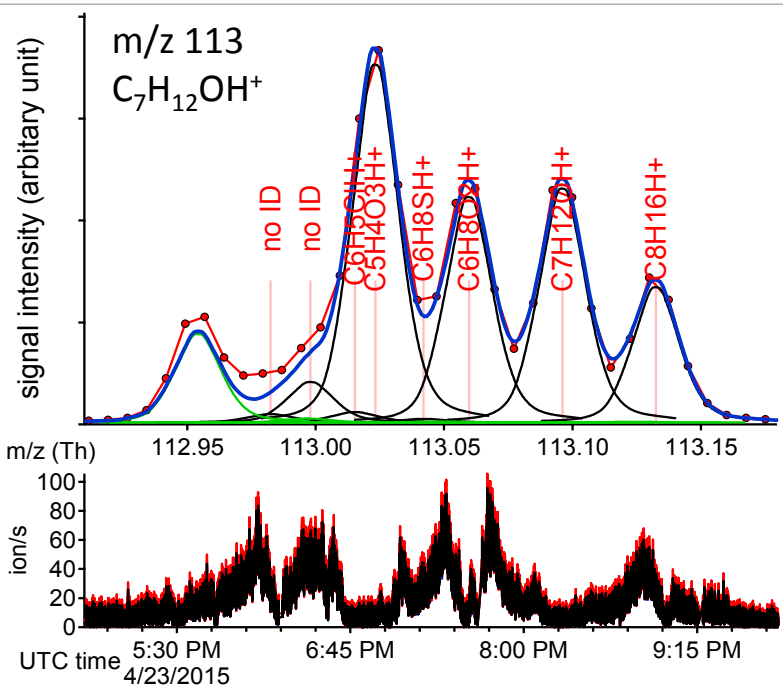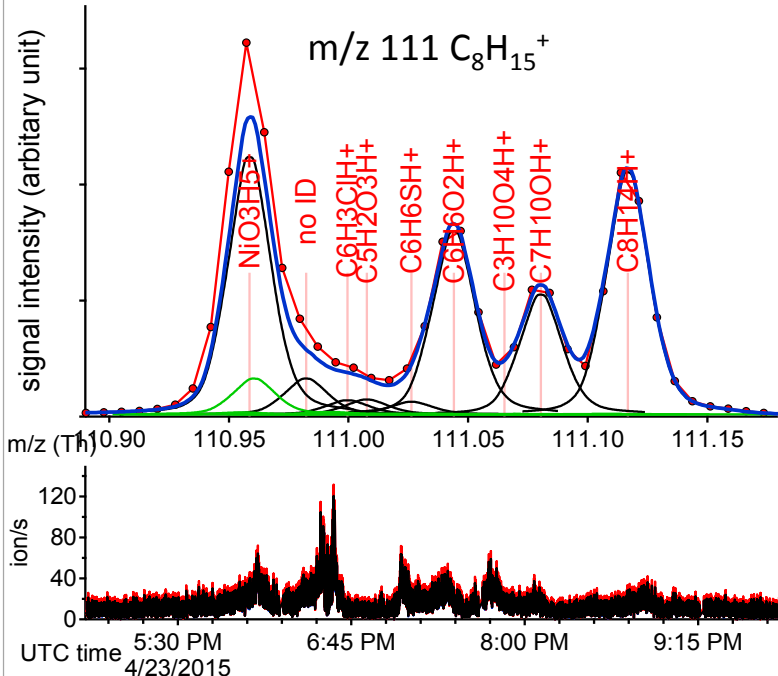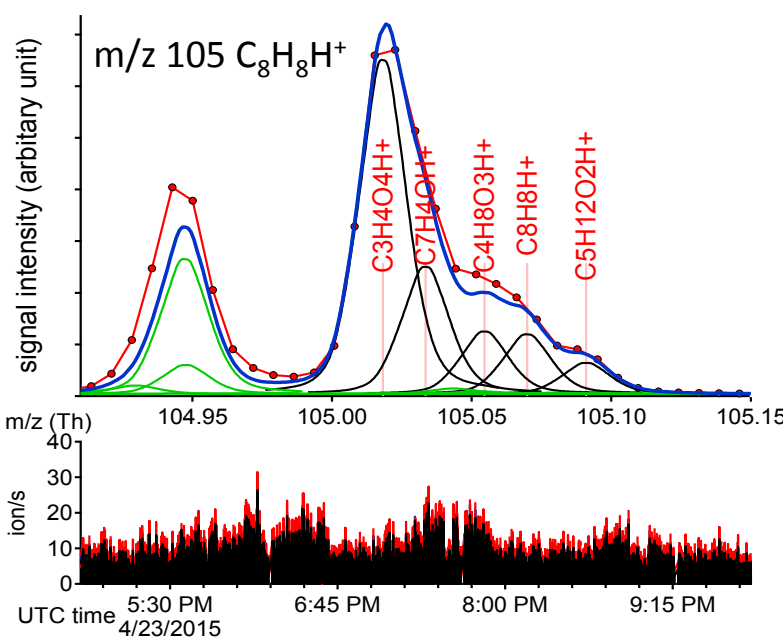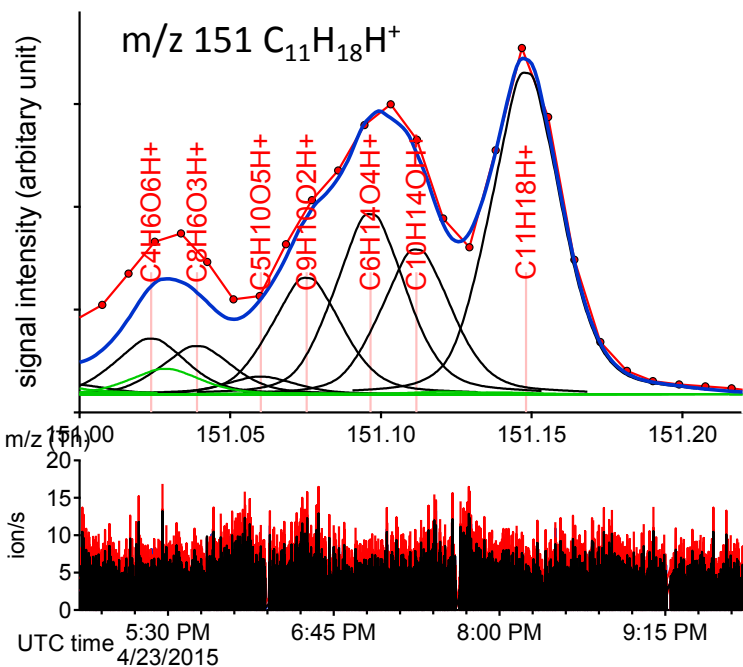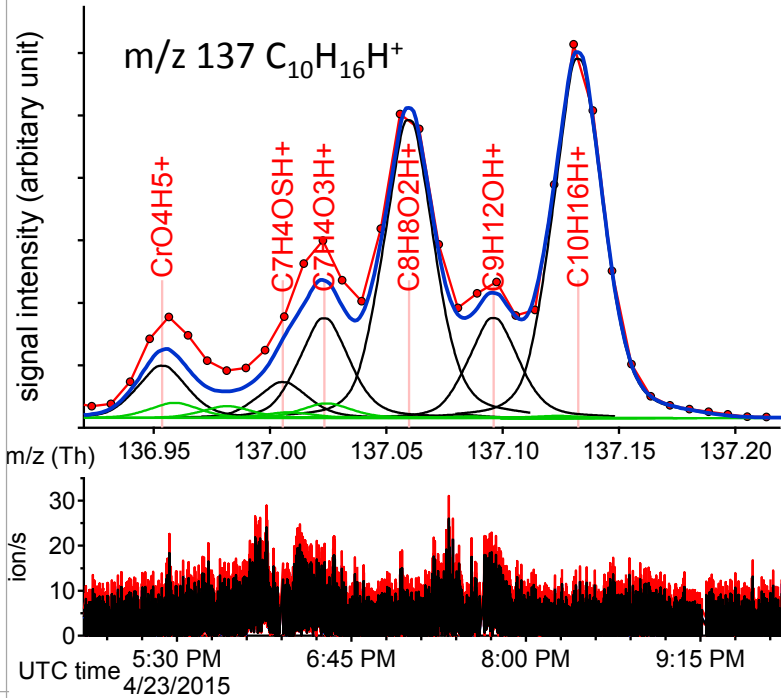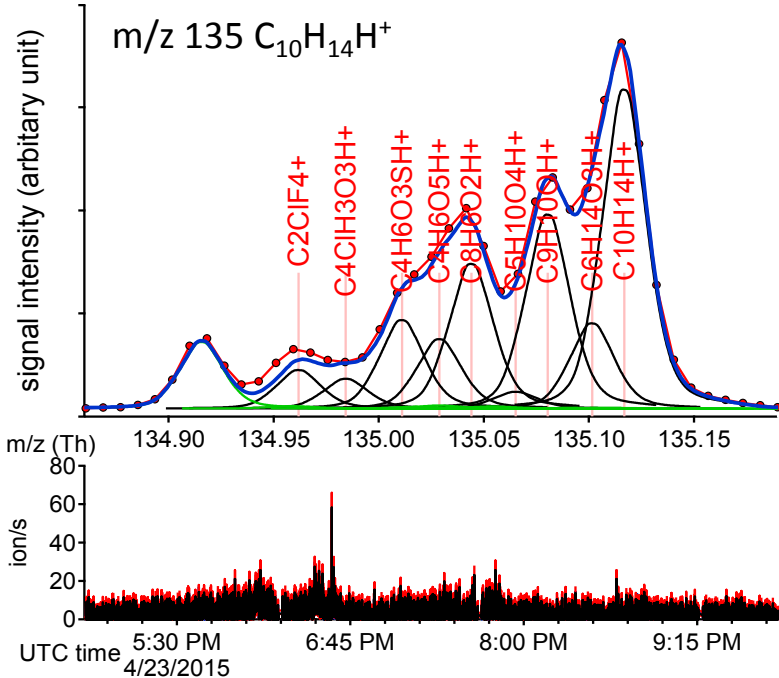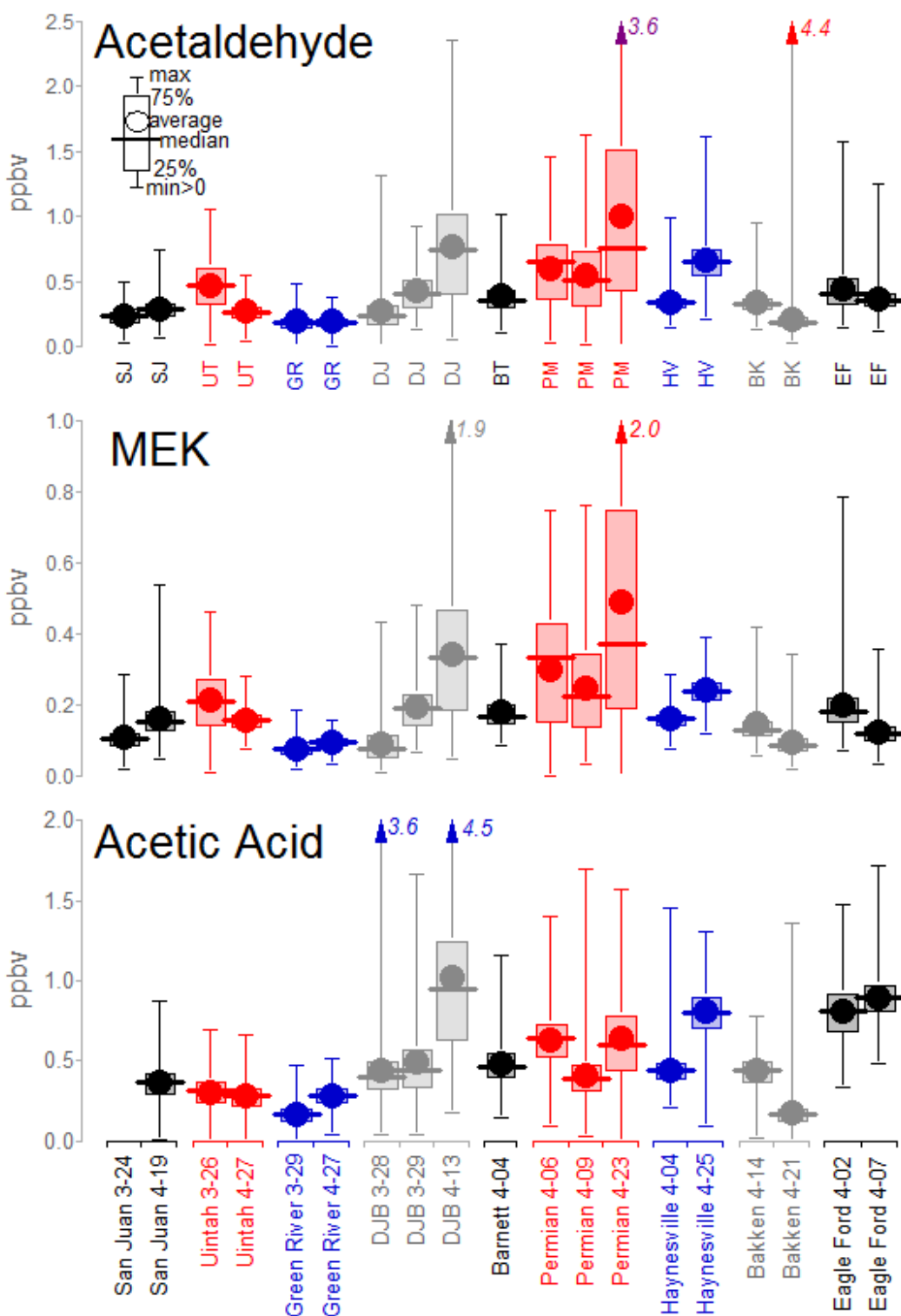
Figure SI 5

Distribution of acetaldehyde, acetone, MEK, and acetic acid during each flight.

Figure SI 6
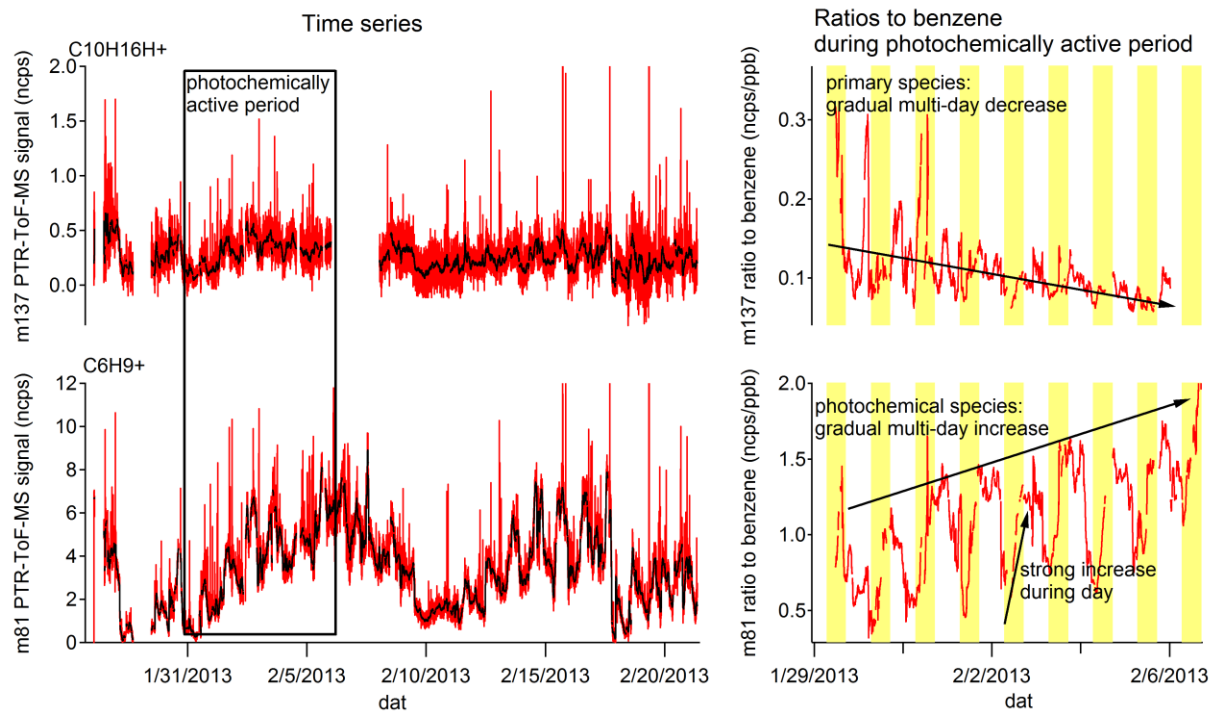
PTR-ToF-MS measurement of m/z 137 $C_{10}H_{16}H^+$ and m/z 81 $C_6H_9^+$ during the UBWOS 2013 campaign in the Uintah oil and gas field, Utah. The right two panels show the ion ratios to benzene, which indicate whether they belong to primary or photochemically produced species. We note that frequently, m/z 137 $C_{10}H_{16}H^+$ is interpreted as monoterpenes, and m/z 81 $C_6H_9^+$ as a monoterpene fragment (e.g. Kim et al. (2010)). In both Utah (UBWOS 2013) and the Permian (SONGNEX 2015) these two masses are uncorrelated, and m/z 81 has much higher intensity than m/z 137.

Figure SI 7
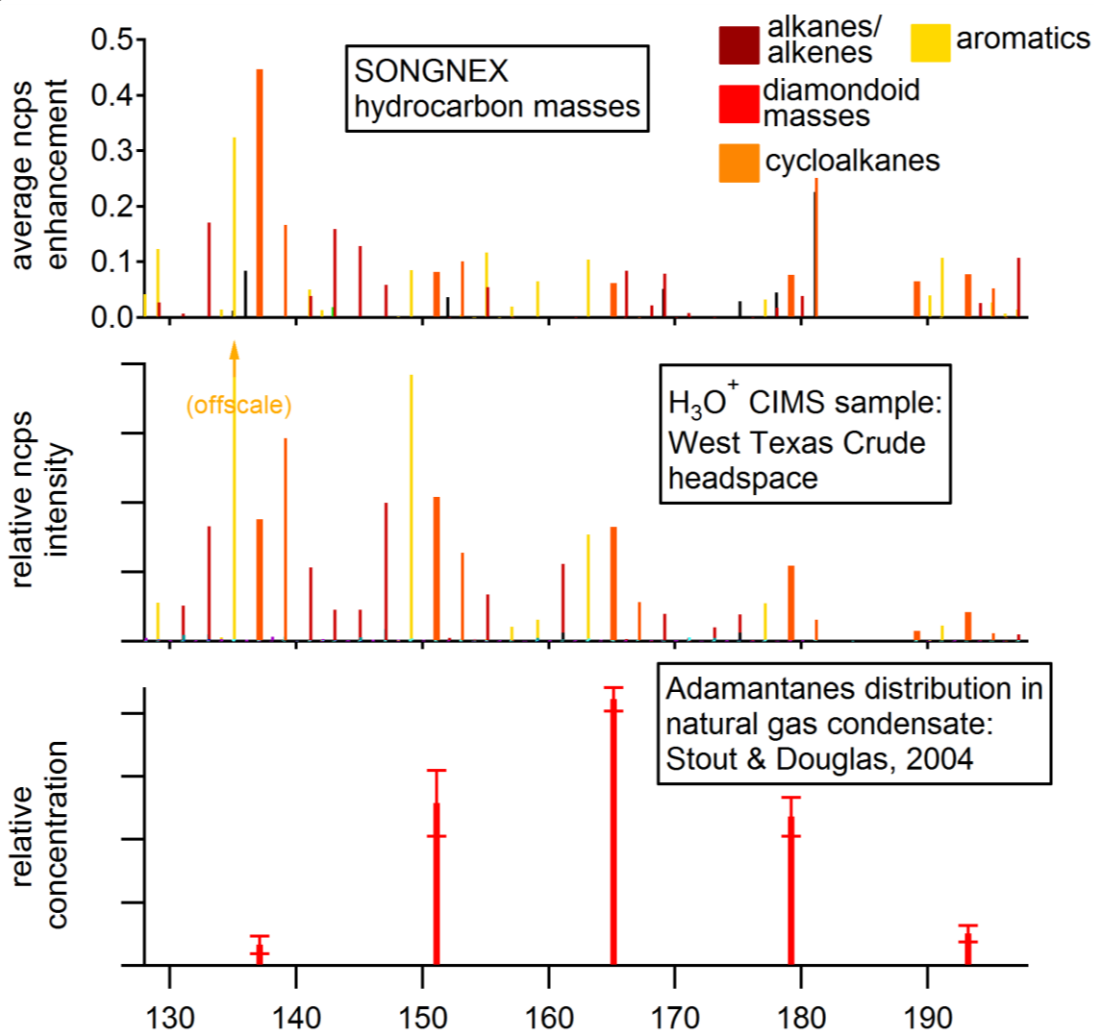
Potential diamondoid ion masses in SONGNEX measurement (top), headspace of West Texas Crude (middle), compared to reported distribution of diamondoids (bottom) (Stout and Douglas, 2004). Diamondoid masses are the bold sticks in the mass spectra. The three distributions are somewhat different. This could be because: (1) the $C_{10}H_{16}H^+$ detected during SONGNEX is not a diamondoid; (2) inlet effects reduced the measured amount of higher molecular weight species; (3) distribution of diamondoids in other fuels can differ from that presented by Stout and Douglas (2004); (4) The higher molecular weight species have a shorter atmospheric lifetime.

Figure SI 8
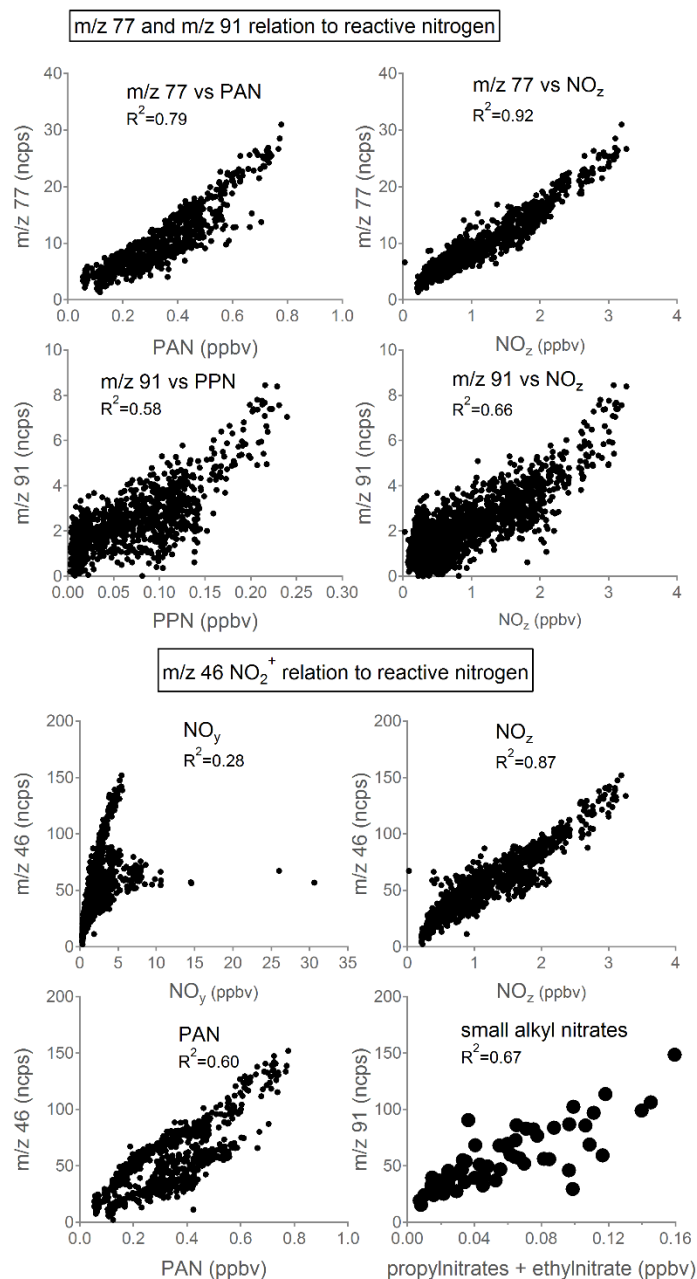
Comparison of H_3O^+ ToF-CIMS masses m/z 77 $C_2H_4O_3H^+$, m/z 91 $C_3H_6O_3H+$, and m/z 46 NO_2^+ to various reactive nitrogen species during the April 23 SONGNEX flight. Ten-second average data is shown for clarity. For the comparison to small alkyl nitrates, the H_3O^+ ToF-CIMS data has been averaged to the iWAS sampling times. Small differences exist between the CaRDS and Chemiluminescence measurements; these were averaged where both were available. The choice of NO_x and NO_y data source does not affect our conclusions.

Figure SI 9.
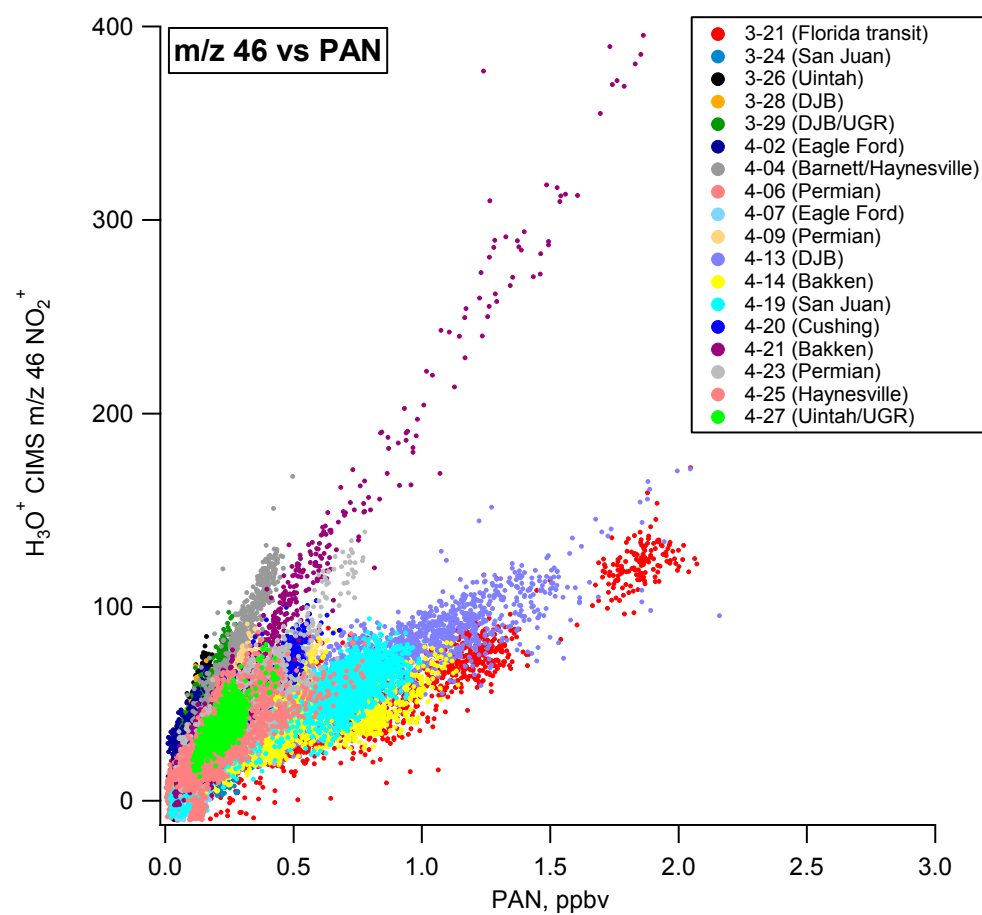
H₃O⁺ ToF CIMS m/z 46 NO₂⁺ tracer measurements compared to PAN. The high m/z 46 during the 4-21 Bakken flight was within an aged biomass burning plume (identified by enhanced acetonitrile).

Figure SI 10
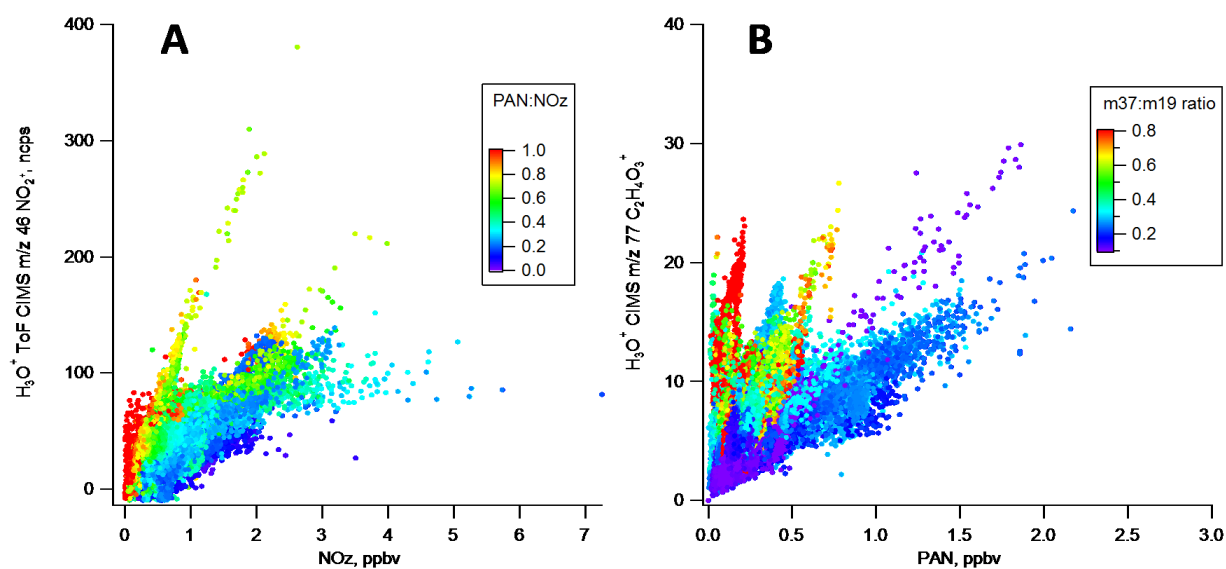
A: H_3O^+ ToF-CIMS m/z 46 compared to NO_z from all flights, colored by the fraction of NO_z accounted for by PAN. B: H_3O^+ ToF-CIMS m/z 77 compared to PAN from all flights, colored by relative humidity proxy m/z 37 $H_5O_2^+$:m/z19 H_3O^+.

Figure SI 11
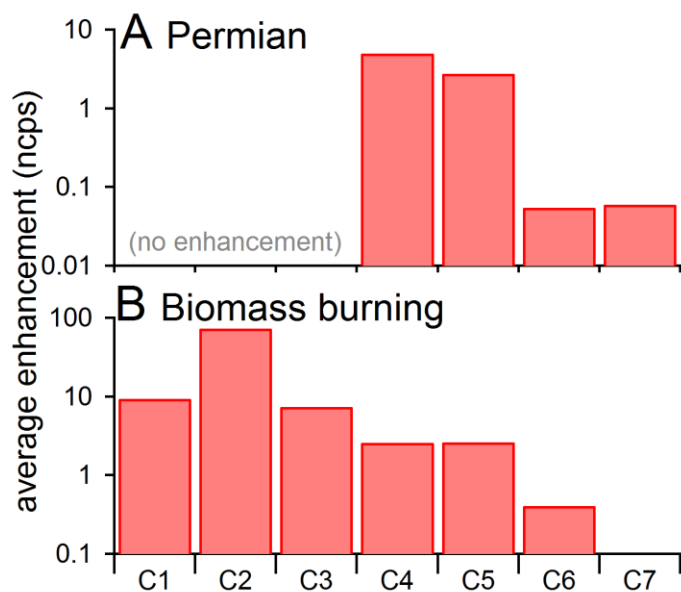
Comparison of the distribution of unsaturated nitrogen species $C_xH_{2x-1}NH^+$ between (a) oil- and gas-related VOCs measured during the April 23 Permian flight, and (b) a biomass burning plume encountered during the April 21 Bakken flight. The series is m/z 28 $HCNH^+$, m/z 42 $C_2H_3NH^+$, m/z 56 $C_3H_5NH^+$, m/z 70 $C_4H_7NH^+$, etc. The values shown are the average signal enhancement (ncps enhancement) in the boundary layer during the Permian flight, and the average signal enhancement (ncps enhancement) in the biomass burning plume compared to immediately before the plume during the Bakken flight.

Figure SI 12
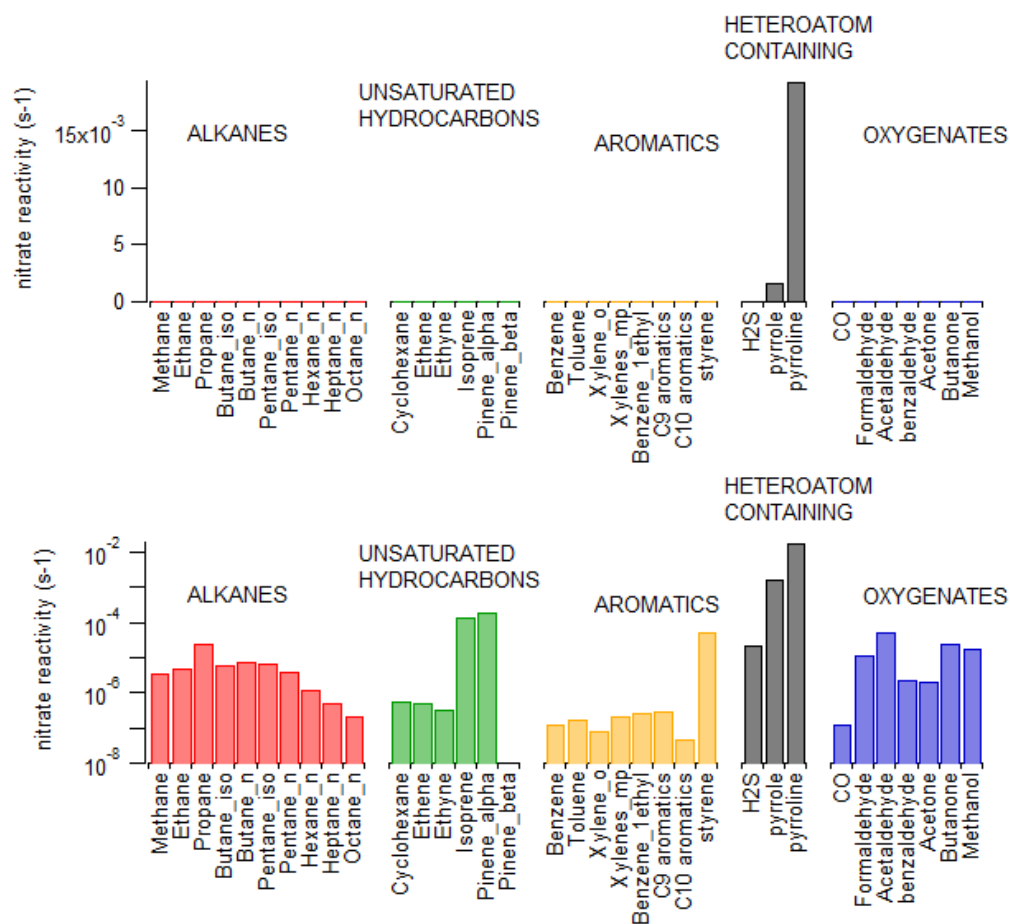
Scaled nitrate reactivity of measured species. Top: linear scale. Bottom: log scale. NO_3 rate constants from Atkinson and Arey (2003), Atkinson et al. (1985), Atkinson et al. (2006), Atkinson (1991), DeMore et al. (1997), Chew et al. (1998).

S4. Comparison of nitrate reactivity to literature

The estimated average pyrroline nitrate reactivity is 15×10^{-3} s^{-1} (assuming the same nitrate reaction constant as pyrrole).

For comparison, Stutz et al. (2010) measured nocturnal nitrate loss rates in Houston, TX in an area influenced by emissions from the petrochemical industry. Total nitrate loss frequency was typically around 20 to 60 $\times10^{-3}$ s^{-1} during the middle of the night. VOC nitrate reactivity ranged from 0 to 50×10^{-3} s^{-1} and was typically the dominant loss mechanism. Indirect loss via N_2O_5 uptake to aerosol was the second most important pathway and ranged from 0 to 40 $\times10^{-3}$ s^{-1}.

Crowley et al. (2011) measured nocturnal nitrate loss frequency in polluted air in Spain. Total nitrate loss frequency was on the order of 5×10^{-3} s^{-1} to 50×10^{-3} s^{-1}. Loss of NO_3 to VOCs, and loss via N_2O_5 uptake to aerosol were both important loss mechanisms, each on the order of 5×10^{-3} s^{-1}.

Conversely, (Tsai et al., 2014) found that loss via N_2O_5 uptake to aerosol accounted for nearly all of the typically 50 $\times10^{-3}$ s^{-1} NO_3 loss in the Los Angeles metropolitan area.

References

US Energy Information Administration: Drilling Productivity Report, 2016.

Atkinson, R., Aschmann, S. M., Winer, A. M., and Carter, W. P. L.: Rate constants for the gas-phase reactions of nitrate radicals with furan, thiophene, and pyrrole at 295 .+-. 1 K and atmospheric pressure, Environ. Sci. Technol., 19, 87-90, 10.1021/es00131a010, 1985.

Atkinson, R.: Kinetics and Mechanisms of the Gas‐Phase Reactions of the NO3 Radical with Organic Compounds, J. Phys. Chem. Ref. Data, 20, 459-507, 10.1063/1.555887, 1991.

Atkinson, R., and Arey, J.: Atmospheric degradation of volatile organic compounds, Chem. Rev., 103, 4605-4638, 2003.

Atkinson, R., Baulch, D., Cox, R., Crowley, J., and Hampson Jr, R.: Summary of evaluated kinetic and photochemical data for atmospheric chemistry, IUPAC Subcommittee on Gas Kinetic Data Evaluation for Atmospheric Chemistry, 2006.

Bertram, T. H., Kimmel, J. R., Crisp, T. A., Ryder, O. S., Yatavelli, R. L. N., Thornton, J. A., Cubison, M. J., Gonin, M., and Worsnop, D. R.: A field-deployable, chemical ionization time-of-flight mass spectrometer, Atmos. Meas. Tech., 4, 1471-1479, 10.5194/amt-4-1471-2011, 2011.

Chew, A. A., Atkinson, R., and Aschmann, S. M.: Kinetics of the gas-phase reactions of NO3 radicals with a series of alcohols, glycol ethers, ethers and chloroalkenes, J. Chem. Soc. Faraday T., 94, 1083-1089, 10.1039/A708183I, 1998.

Corbin, J. C., Othman, A., Haskins, J. D., Allan, J. D., Sierau, B., Worsnop, D. R., Lohmann, U., and Mensah, A. A.: Peak fitting and integration uncertainties for the Aerodyne Aerosol Mass Spectrometer, Atmos. Meas. Tech. Discuss., 8, 3471-3523, 10.5194/amtd-8-3471-2015, 2015.

Crowley, J. N., Thieser, J., Tang, M. J., Schuster, G., Bozem, H., Beygi, Z. H., Fischer, H., Diesch, J. M., Drewnick, F., Borrmann, S., Song, W., Yassaa, N., Williams, J., Pöhler, D., Platt, U., and Lelieveld, J.: Variable lifetimes and loss mechanisms for NO3 and N2O5 during the DOMINO campaign: contrasts between marine, urban and continental air, Atmos. Chem. Phys., 11, 10853-10870, 10.5194/acp-11-10853-2011, 2011.

Cubison, M. J., and Jimenez, J. L.: Statistical precision of the intensities retrieved from constrained fitting of overlapping peaks in high-resolution mass spectra, Atmos. Meas. Tech., 8, 2333-2345, 10.5194/amt-8-2333-2015, 2015.

de Gouw, J. A., Middlebrook, A. M., Warneke, C., Goldan, P. D., Kuster, W. C., Roberts, J. M., Fehsenfeld, F. C., Worsnop, D. R., Canagaratna, M. R., Pszenny, A. A. P., Keene, W. C., Marchewka, M., Bertman, S. B., and Bates, T. S.: Budget of organic carbon in a polluted atmosphere: Results from the New England Air Quality Study in 2002, J. Geophys. Res.: Atmos., 110, D16305, 10.1029/2004JD005623, 2005.

DeMore, W. B., Sander, S. P., Golden, D., Hampson, R., Kurylo, M. J., Howard, C. J., Ravishankara, A., Kolb, C., and Molina, M.: Chemical kinetics and photochemical data for use in stratospheric modeling. evaluation no. 12, NASA Panel for Data Evaluation, 1997.

Kim, S., Karl, T., Guenther, A., Tyndall, G., Orlando, J., Harley, P., Rasmussen, R., and Apel, E.: Emissions and ambient distributions of Biogenic Volatile Organic Compounds (BVOC) in a ponderosa pine ecosystem: interpretation of PTR-MS mass spectra, Atmos. Chem. Phys., 10, 1759-1771, 10.5194/acp-10-1759-2010, 2010.

Koss, A. R., de Gouw, J., Warneke, C., Gilman, J. B., Lerner, B. M., Graus, M., Yuan, B., Edwards, P., Brown, S. S., Wild, R., Roberts, J. M., Bates, T. S., and Quinn, P. K.: Photochemical aging of volatile organic compounds associated with oil and natural gas extraction in the Uintah Basin, UT, during a wintertime ozone formation event, Atmos. Chem. Phys., 15, 5727-5741, 10.5194/acp-15-5727-2015, 2015.

Müller, M., George, C., and D'Anna, B.: Enhanced spectral analysis of C-TOF Aerosol Mass Spectrometer data: Iterative residual analysis and cumulative peak fitting, Int. J. Mass Spectrom. , 306, 1-8, http://dx.doi.org/10.1016/j.ijms.2011.04.007, 2011.

Stark, H., Yatavelli, R. L. N., Thompson, S. L., Kimmel, J. R., Cubison, M. J., Chhabra, P. S., Canagaratna, M. R., Jayne, J. T., Worsnop, D. R., and Jimenez, J. L.: Methods to extract molecular and bulk chemical information from series of complex mass spectra with limited mass resolution, 389, 26-38, http://dx.doi.org/10.1016/j.ijms.2015.08.011, 2015.

Stout, S. A., and Douglas, G. S.: Diamondoid Hydrocarbons—Application in the Chemical Fingerprinting of Natural Gas Condensate and Gasoline, Environ. Forensics, 5, 225-235, 10.1080/15275920490886734, 2004.

Stutz, J., Wong, K. W., Lawrence, L., Ziemba, L., Flynn, J. H., Rappenglück, B., and Lefer, B.: Nocturnal NO3 radical chemistry in Houston, TX, Atmos. Environ., 44, 4099-4106, http://dx.doi.org/10.1016/j.atmosenv.2009.03.004, 2010.

Timonen, H., Cubison, M., Aurela, M., Brus, D., Lihavainen, H., Hillamo, R., Canagaratna, M., Nekat, B., Weller, R., Worsnop, D., and Saarikoski, S.: Applications and limitations of constrained high-resolution peak fitting on low resolving power mass spectra from the ToF-ACSM, Atmos. Meas. Tech., 9, 3263-3281, 10.5194/amt-9-3263-2016, 2016.

Tsai, C., Wong, C., Hurlock, S., Pikelnaya, O., Mielke, L. H., Osthoff, H. D., Flynn, J. H., Haman, C., Lefer, B., Gilman, J., de Gouw, J., and Stutz, J.: Nocturnal loss of NOx during the 2010 CalNex-LA study in the Los Angeles Basin, J. Geophys. Res. Atmos. , 119, 13,004-013,025, 10.1002/2014JD022171, 2014.

Warneke, C., McKeen, S. A., de Gouw, J. A., Goldan, P. D., Kuster, W. C., Holloway, J. S., Williams, E. J., Lerner, B. M., Parrish, D. D., Trainer, M., Fehsenfeld, F. C., Kato, S., Atlas, E. L., Baker, A., and Blake, D. R.: Determination of urban volatile organic compound emission ratios and comparison with an emissions database, J. Geophys. Res., 112, 10.1029/2006jd007930, 2007.